

Client Report 2000/53

**Probabilistic Seismic
Hazard Assessment
of New Zealand:**

**New Active Fault
Data
Seismicity Data
Attenuation
Relationships and
Methods**

Authors

Mark Stirling
Graeme McVerry
Kelvin Berryman
Peter McGinty
Pilar Villamor
Russ Van Dissen
David Dowrick
Jim Cousins
Rupert Sutherland

May 2000



Institute of
**GEOLOGICAL
& NUCLEAR
SCIENCES**
Limited



Institute of
**GEOLOGICAL
& NUCLEAR
SCIENCES**
Limited

Probabilistic Seismic Hazard Assessment of New Zealand:

New Active Fault Data, Seismicity Data, Attenuation Relationships and Methods

Mark Stirling, Graeme McVerry, Kelvin Berryman, Peter McGinty,
Pilar Villamor, Russ Van Dissen, David Dowrick, Jim Cousins and Rupert Sutherland

Prepared for

EARTHQUAKE COMMISSION RESEARCH FOUNDATION

**Institute of Geological & Nuclear Sciences client report 2000/53
Project Number 41984B.10**

May 2000



EXECUTIVE SUMMARY

We present the results of a new probabilistic seismic hazard analysis (PSHA) for New Zealand. The PSHA incorporates geological data describing the location and earthquake recurrence behaviour of 305 active faults, a seismicity catalogue with greatly improved locations for many events, new attenuation relationships for peak ground acceleration and spectral acceleration developed specifically for New Zealand, and state-of-the-art PSH methodology developed in New Zealand and the USA. The methodology and data used in the PSHA builds on the data and methods used in an experimental PSHA of New Zealand by Stirling et al. (1998), and supersedes the PSHAs of Matuschka et al. (1985) and Smith and Berryman (1983, 1986), which were largely based on the historical record of earthquakes (historical recording began with European settlement in 1840). These models served as the basis for the current New Zealand Loadings Standard NZS4203:1992 (Standards New Zealand, 1992). PSH maps produced from our new model show the highest hazard to occur in Fiordland (vicinity of the Fiordland subduction zone and the offshore extent of the Alpine Fault), along the axial tectonic belt (Westland, Marlborough, north Canterbury, Wellington, Wairarapa, western Hawkes Bay and eastern Bay of Plenty), the Taupo Volcanic Zone (TVZ, a zone of active crustal extension and volcanism running from the central North Island volcanoes to the Bay of Plenty), and in the seismically active area of north Westland/southwest Nelson (area of the Buller and Inangahua earthquakes). The maps show generally similar patterns of hazard to the maps of Stirling et al (1998), but very different patterns to those shown on the maps of Smith and Berryman (1983, 1986) and Matuschka et al. (1985). The largest differences exist in the vicinity of the major active faults, which generally have not produced large earthquakes in historic time, but have produced them abundantly in prehistoric time.

Examination of the PSHA at the major population centres reveals that they have the following rank in decreasing order of hazard; Wellington, Christchurch, Dunedin and Auckland. The hazard is highest in Wellington, since it is close to a number of major active faults, and within an area of high seismicity in historical time. In comparison, the other centres are generally located in areas away from the major active faults, and in areas of relatively low seismicity rates.



CONTENTS

EXECUTIVE SUMMARY	I
1.0 INTRODUCTION.....	1
1.1 GENERAL	1
1.2 REVIEW OF THE 1985 HAZARD MODEL	2
2.0 NEOTECTONICS AND HISTORICAL SEISMICITY	4
3.0 PROBABILISTIC SEISMIC HAZARD ANALYSIS.....	6
3.1 METHOD AND ANALYSIS	6
3.2 EARTHQUAKE SOURCES.....	6
3.2.1 <i>Faults</i>	6
3.2.2 <i>Distributed Earthquake Sources</i>	11
3.3 ATTENUATION MODEL	14
3.3.1 <i>Introduction</i>	14
3.3.2 <i>Site Classification</i>	15
3.3.3 <i>Form of the McVerry et al. Model</i>	17
3.4 COMPUTATION OF HAZARD	25
3.5 HAZARD ESTIMATES	26
3.5.1 <i>Hazard Maps</i>	26
3.5.2 <i>Site Specific Hazard</i>	28
4.0 SUMMARY AND CONCLUSIONS	33
5.0 FUTURE DEVELOPMENTS AND SENSITIVITY STUDIES	34
6.0 ACKNOWLEDGMENTS	37
7.0 REFERENCES.....	38



FIGURE CAPTIONS

- Figure 1:** The plate tectonic setting of New Zealand. The country is divided into the neotectonic provinces identified by Berryman and Beanland (1988).
- Figure 2:** The 305 active fault sources used as input for the PSHA. The numbers beside each fault correspond to the index numbers given in the fault table (Appendix 1).
- Figure 3:** The distribution of shallow crustal seismicity in New Zealand (a), and the deeper seismicity of the Fiordland and Hikurangi subduction zones (b). The seismotectonic zones we have defined to sort the catalogue, assign initial regional maximum cutoff magnitudes (M_{cutoff}), and calculate parameter b of the Gutenberg-Richter relationship for seismicity are shown in (a). In the case of (b), many of the deep zones overlap in plan view, so we show the seismicity of each zone as a particular colour, rather than trying to colour-code the actual zones. The vertical extents of the seismotectonic zones have been defined from the spatial and depth distribution of seismicity, and are shown on each plot as a depth range beside the zone number (e.g. "z20 10-45 km" indicates that zone 20 has a depth range of 10 to 45 km). Since the crustal and deep sources have been defined at different scales, the lower-depth-limit of a crustal zone sometimes overlaps with the upper-depth-limit of a deep zone. In these cases the seismicity parameters calculated for the crustal zones are assumed to represent the seismicity of the overlapping areas. In (c) we show the seismicity for the three different time periods of completeness for events of all depths from 1900 to 1997, and cross sections of seismicity across and beneath the country. See the locations of the cross sections on the "Magnitude 6.5" map. Cross sections are oriented with the northwest end to the left of the page. Maps and cross sections in (c) are taken from McGinty (1999).
- Figure 4:** Contours of (a)-(e) the maximum-likelihood cumulative number of events per year for $M \geq 4$, calculated from three catalogue completeness levels and magnitudes ($M \geq 4$ since 1964, $M \geq 5$ since 1940, and $M \geq 6.5$ since 1840); (f)-(j) parameter b of the Gutenberg-Richter relationship $\text{Log}N = A - bM$, and; (k) the maximum "cutoff" magnitude (M_{cutoff}) assumed for distributed earthquakes, for various depth layers beneath the country. The contours have been made over a gridwork of N , b and M_{cutoff} that have been smoothed with a Gaussian smoothing function, in which the correlation distance (standard deviation) is set to 50 km. Since M_{cutoff} for all of the deep seismotectonic zones is set to 7, we only show a contour plot of M_{cutoff} for the crustal (20 km) depth layer. Note that white areas on the b value plots are where no seismicity exists in the depth range shown.
- Figure 5:** (a)-(f). Probabilistic seismic hazard maps for New Zealand for site class B (intermediate soil). The maps show the levels of p_{ga} and 5% damped response spectral acceleration (0.2 and 1s period) with return periods of 475 years (i.e. 10% probability in 50 years) and 1000 years (10% probability in 105 years).
- Figure 6:** Seismic hazard curves for site class B of the annual rate of exceedance for various levels of p_{ga} (a), and 5% damped response spectral acceleration (1s period; b) at the centres of Auckland, Wellington, Christchurch, Dunedin and Otira. Otira is included in the plots as a useful comparison to the main centres, since it is located in the area of highest hazard in the country (Fig. 5).
- Figure 7:** Response spectra for Auckland, Wellington, Christchurch, Dunedin and Otira, for 475 and 1000 year return periods for site class B.
- Figure 8:** Disaggregation plots for Auckland, Wellington, Christchurch, Dunedin and Otira. The plots show the percentage contribution to the 475 and 1000 year levels of hazard (Fig. 7) of the various magnitudes and source-to-site distances of earthquake sources in the model. The plots are produced for p_{ga} and 1s spectral accelerations for site class B.
- Figure 9:** Comparison of the 475 year return period spectra for the five centres obtained in this study (NHM), and the Matuschka et al. (1985) study, and by using the modified Katayama attenuation model of the 1985 study with our NHM seismicity model.



1.0 INTRODUCTION

1.1 General

In this report we present the results of a probabilistic seismic hazard analysis (PSHA) for New Zealand that represents a significant improvement on earlier national PSHAs. In our analysis, we combine geologic data describing the geometry and activity of 305 major active earthquake faults (locations, fault lengths, fault type, slip rates, single event displacements, estimated magnitudes, and average recurrence intervals), and combine these data with historical seismicity data to develop PSH maps for the country. Our approach is to use the geologic data and historical observations of large earthquakes to estimate the locations, magnitudes, and recurrence rates of future large earthquakes. We then use historical seismicity data (earthquake data recorded instrumentally since 1940, and earthquake data derived largely from interpretation of felt intensity data over the period 1840-1940; magnitude scales used are a mixture of moment magnitude, M_w , local magnitude, M_L and surface wave magnitudes M_S) to estimate the locations, magnitudes, and recurrence rates of moderate-to-large "distributed" earthquakes in and around the mapped faults. Our PSH maps show the peak ground accelerations (pga) and 5% damped response spectral accelerations (SA) for 0.2s and 1s periods, (often referred to as "SA(0.2s)" and "SA(1s)") expected for return periods of 475 years (i.e. 10% probability in 50 years) and 1000 years (i.e. 10% probability in 105 years) at average soil sites (Class B site conditions of Standards New Zealand, 1992).

The prime motivation for our study is that the existing national PSH maps are now out of date in terms of the methodology and data used to estimate hazard. The widely used national seismic hazard maps of Matuschka et al. (1985) and Smith and Berryman (1983, 1986) were largely based on the historical record of earthquakes, and did not explicitly incorporate geological data. More recently, national PSH maps have been published that incorporate both geological and historical seismicity data, and new methods for the treatment of historical seismicity (Stirling et al., 1998), but these maps used an unpublished interim version of the current attenuation model, and preliminary versions of the fault database and historical earthquake catalogue. Our PSHA is developed from the Stirling et al. PSHA, with improvements to the treatment of historical seismicity, the introduction of new ground motion attenuation relationships for New Zealand to the model, and use of a much enlarged and revised active fault database. These are new data describing the earthquake recurrence behaviour of active faults in New Zealand, largely collected by GNS, and the Natural Hazards Research Centre of the University of Canterbury (Pettinga et al., 1998). Furthermore, the locations and magnitudes of many earthquakes in the historical catalogue have been refined for use in this study (McGinty 1999).



1.2 Review of the 1985 hazard model

The Matuschka et al. (1985) seismic hazard study served as the basis for the current New Zealand Loadings Standard NZS4203:1992 (Standards New Zealand, 1992). It made use of a seismicity model developed by Smith and Berryman (1983, 1986) and a Japanese response spectrum attenuation model developed by Katayama (1982) and modified for New Zealand conditions. When the hazard analysis was published in 1985, it was one of the earliest applications of uniform hazard spectra as the basis for developing code loadings. The Matuschka et al. model grew out of earlier work at the University of Canterbury (Peek et al., 1980; Mulholland, 1982).

The seismicity model divided New Zealand into a number of regional source zones of uniformly distributed seismicity, each characterised by a rate parameter a_4 (the annual number of earthquakes per 1000 km² exceeding magnitude 4), a b-value, and a maximum magnitude M_{max} . These parameters were derived primarily from an analysis of historical seismicity, with some ad hoc adjustment on the basis of geological input. There was no explicit modelling of faults in the model. However, the maximum magnitudes were usually assigned from geological input on the magnitudes estimated for active faults in each region.

The response spectrum attenuation model specified the spectral values for each period as a product of a magnitude term, a distance term and a site class term. The magnitude and distance terms were defined for five magnitude classes (4.5-5.3, 5.4-6.0, 6.1-6.7, 6.8-7.4 and 7.5-7.9), and five distance classes (0-19 km, 20-59 km, 60-119 km, 120-199 km and 200-405 km). The distance factors were modified in such a way that effectively no site was closer than 20 km to an earthquake source. These modifications to the attenuation relation, and the lack of active fault sources in the model, meant that there was no increase in the estimated hazard within the immediate vicinity of major active faults. This process led to a significant underestimation of the hazard adjacent to the most active fault systems.

The Katayama model used four site classes, although two of these were usually combined in Japanese practice. These three remaining site classes were interpreted for New Zealand conditions as the three site subsoil categories adopted in NZS42032:1992, namely: (a) rock or very stiff soil sites; (b) intermediate soil sites; and (c) flexible or deep soil sites.

The hazard results were presented in terms of contour maps of the 5% damped response spectrum acceleration at 0.2s, SA(0.2s), for Katayama's ground class III, corresponding to the intermediate soil category of NZS4203:1992. The contour maps were formed from estimates obtained for a 0.5° by 0.5° grid spacing throughout the country. The value at 0.2s usually corresponded to the peak of the uniform hazard



spectrum for a given return period. The 450 year return period map was adopted for the zone factor Z in the code, apart from limitation of the range to 0.6g to 1.2g rather than the calculated range of 0.3g to 1.3g. The adoption of a Z value of 0.6g for the lower seismicity region of the country around Auckland and in Northland imposed considerable conservatism in this region on the estimates derived directly from the hazard analysis.



2.0 NEOTECTONICS AND HISTORICAL SEISMICITY

New Zealand straddles the boundary of the Australian and Pacific plates, where relative plate motion is obliquely convergent across the plate boundary at about 50 mm/yr at the latitude of East Cape, 40 mm/yr at the latitude of central New Zealand, and 35 mm/yr in the Fiordland area (De Mets et al. 1994; Fig. 1). The relative plate motion is expressed in New Zealand by the presence of numerous active faults (Fig. 2), and a high rate of small-to-moderate ($M < 7$) earthquakes (Fig. 3), including the occurrence of many large earthquakes ($M 7-7.9$) and one great earthquake ($M > 8$) in historic time. The historic record of $M \geq 6.5$ earthquakes dates from 1840, which was the time that European settlement began in New Zealand. A southeast-dipping subduction zone lies at the far southwestern end of the country ("Fiordland subduction zone" in Fig. 1), and this is linked to a major northwest-dipping subduction zone in the eastern North Island ("Hikurangi subduction zone" in Fig. 1) by a 1000 km long zone of dextral oblique slip faults ("Axial tectonic belt" in Fig. 1). The majority of the relative plate motion is accommodated by the faults of the axial tectonic belt in the area between the Fiordland and Hikurangi subduction zones.

The Hikurangi subduction interface dips beneath the eastern North Island, and abrupt changes in the spatial and depth distribution of seismicity along the subduction interface (Fig. 3) have been suggested as marking "tears" or segment boundaries in the subduction zone (Reyners, 1983, 1998). However, only one large earthquake, and no great earthquakes are known to have been produced by the Hikurangi subduction interface in historic time (since 1840), so that little is known about the earthquake potential of this feature. The Fiordland subduction zone dips southeast offshore from Fiordland, and is steeply dipping beneath Fiordland. The Fiordland subduction interface also shows abrupt changes in seismicity patterns along strike, and the lateral extent of the aftershock zone of a recent large earthquake (the $M 7$, 1993 August 10 Fiordland earthquake; Van Dissen et al. 1994) shows that rupture lengths less than the length of the entire subduction zone do occur. Some of the highest rates of seismicity in the country occur within the subducted plates of the subduction zones. High rates of moderate earthquakes also occur above the Fiordland subduction zone, and to a lesser extent above the Hikurangi subduction zone.

The axial tectonic belt is a zone of dextral transpression, most dramatically illustrated by the southern section of the Alpine Fault (Fig. 1), where dextral slip rates of 26 ± 7 mm/yr are observed (Berryman & Beanland, 1988; Berryman et al. 1992; Sutherland & Norris, 1995). The Alpine Fault accommodates a large portion of the relative plate motion in the central South Island, but the fault has not produced any large or great earthquakes in historic time. It is presently characterised by low rates of seismicity. Geologic data provide evidence for the occurrence of great earthquakes on the Alpine Fault with return times of hundreds of years.



Plate motion is distributed across a number of parallel faults with slip rates > 1 mm/yr in the axial tectonic belt of the northern South Island (the Marlborough faults), and across faults and the Hikurangi subduction zone in the southern and eastern North Island (Fig. 1). Faults in the axial tectonic belt show strike-slip, dip-slip and oblique-slip motion. Many moderate or larger earthquakes have occurred within the axial tectonic belt in historic time, including the two largest historical earthquakes (the M_w 8.1-8.2, 1855 Wairarapa earthquake, and M_w 7.8 Napier earthquake).

The Taupo Volcanic Zone (Fig. 1) is a zone of active crustal extension that has developed in response to the southward migration of back arc spreading from the Havre Trough (Fig. 1) into the continental margin of New Zealand in the last two million years (Cole & Lewis, 1981). The crustal extension is occurring across the zone at a rate of about 10mm/yr (e.g. Berryman & Beanland, 1988, Villamor and Berryman, in press), and normal faults typically have slip rates of 0.2-1 mm/yr in the zone. Several moderate-sized earthquakes have produced surface ruptures in the Taupo Volcanic Zone (TVZ) in historic time, the most recent being the M_w 6.5, 1987 March 2 Edgecumbe earthquake produced by a normal slip rupture of the Edgecumbe Fault. High rates of small earthquakes also characterise the TVZ.

Faults located away from the axial tectonic belt and TVZ tend to have slip rates that are about an order of magnitude less than the faults in those areas. Reverse faults with slip rates of 0.1 - 1 mm/yr characterise the style of faulting in central Otago and south Canterbury (Fig. 1), and similar slip rates characterise the reverse faults in north Westland and Nelson (Fig. 1). The reverse faults have developed in response to the oblique compression across the plate boundary. The M_w 7.6, 1929 Buller, and M_w 7.2, 1968 Inangahua earthquakes occurred on reverse faults in the Nelson - north Westland area, and high seismicity rates are observed near the epicenters of these earthquakes. The western North Island is a broad zone of relatively stable crust, disrupted only by normal faults in the northeast and southwest (Fig. 1). Several $M \geq 6.5$ earthquakes have occurred within the western North Island in historic time, all in the southwest. Finally, the Canterbury-Chathams platform is an area of stable continental crust that stretches well east of the map boundary in Fig. 1. Very few earthquakes have occurred on the Canterbury-Chathams platform in historic time.



3.0 PROBABILISTIC SEISMIC HAZARD ANALYSIS

3.1 Method and Analysis

The PSHA methodology of Cornell (1968) forms the basis for our analysis. The steps taken to undertake our PSHA are: (1) to use geologic data and the historical earthquake record to define the locations of earthquake sources across and beneath the country, and the likely magnitudes, tectonic type or mechanism, and frequencies of earthquakes that may be produced by each source; and (2) to estimate the ground motions that the sources will produce at a gridwork of sites that cover the entire country. The computation of ground motions in (2) is achieved with a seismic hazard code that is an improved version of the code developed by Stirling et al. (1998). Improvements to the code are in the treatment of "distributed" seismicity for input to the PSHA, and the new ground motion attenuation relationships for New Zealand (McVerry et al., 2000) that are incorporated into the code.

3.2 Earthquake Sources

3.2.1 Faults

We show the 305 fault sources used in our PSHA in Figure 2, and list them in Appendix 1 (note that there is no fault number 220). The values listed are the parameters for each fault that are input to the hazard analysis, together with values given in brackets for the magnitudes M_{\max} and average recurrence intervals that are calculated within the computer code. The fault data are obtained largely from Stirling et al. (1998), from unpublished GNS data held in consulting reports, computer databases, and in recent field notes. The starting point for developing the fault database was a review of the fault database of Stirling et al. (1998) by one of the authors (Van Dissen). The Stirling et al. database was largely developed from published sources, and so did not incorporate most of the unpublished data held at GNS. Van Dissen's review provided new data and references for many faults, particularly faults in the Wellington region (e.g. the Northern Ohariu and Whitemans Valley Faults) and Marlborough (e.g. Clarence and Awatere Faults). Large amounts of unpublished fault data were then extracted from GNS client reports on geologic investigations in the Marlborough, Canterbury, Westland, Otago, Bay of Plenty-Taupo and East Cape regions (Mazengarb et al. 1997; Pettinga et al., 1998; Stirling et al., 1999; Van Dissen et al. 1993; Woodward Clyde & GNS 1999). Finally, numerous unpublished fault data were extracted from computer files, field notes and plate tectonic reconstructions, which improved the coverage of fault sources in the East Cape region (unpublished data of C. Mazengarb), Westland-northwest Canterbury and Taupo-Taihape areas (unpublished data of K. Berryman and P. Villamor) and western Southland (plate boundary model of R. Sutherland).



The fault traces shown on Figure 2 are generalisations of the mapped fault traces. These generalised faults are appropriate for regional scale PSHA. Using the methodology of Stirling et al. (1998) we divide a given fault into more than one source if: (1) geological data and/or the rupture length of a historic earthquake provide evidence for a fault having separate rupture segments (e.g., the Awatere Fault is divided into two sources); or, (2) a fault has wide (>5km) steps in the fault trace. Data bearing on the geometry (e.g., fault dip) and activity (slip rates, single event displacements, and recurrence intervals) of the fault sources are also listed in Appendix 1. Our method of estimating the likely maximum magnitude (“ M_{max} ” in Appendix 1) and recurrence interval of M_{max} earthquakes produced by each fault source in Figure 2 varies according to the quantity and quality of available data for each fault. Where possible, the magnitudes of large historical earthquakes (usually well constrained from instrumental records or from MM intensity data) and lengths of the associated surface ruptures are used to define the M_{max} and length of particular fault sources. If historical observations are unavailable for a fault source, then the next most preferable method of defining M_{max} is to use published estimates of single-event displacements and fault area, and the equations for seismic moment and moment magnitude:

$$M_o = \mu AD \quad (1)$$

and,

$$\log M_o = 16.1 + 1.5M_{max} \quad (2)$$

in which M_o is the seismic moment (in dyne-cm) corresponding to M_{max} , μ is the rigidity modulus of the crust of the Earth, A is the fault area, and D is the single event displacement (equation 1 is from Aki & Richards, 1980, and equation 2 is from Hanks & Kanamori, 1979). To calculate fault area we use the depth to the base of the seismogenic layer (the depth to the base of seismicity recorded in the region surrounding the fault in GNS’s earthquake catalogue) and dip of the fault to estimate the fault width, and estimates of the fault length from the length of surface traces. Lastly, if single-event displacement data are unavailable, then an empirical regression of Wells & Coppersmith (1994) is used to estimate M_{max} from fault rupture area. The average recurrence interval (T) assigned to M_{max} is either: the published estimate from geological investigations; the recurrence interval calculated with the equation

$$T = D/S \quad (3)$$

if a published recurrence interval estimate is unavailable (D is average single-event displacement and S is the fault slip rate); or the recurrence interval calculated with the equation of Wesnousky (1986).



$$T = M_o/M_{orate} \quad (4)$$

if single event displacement data are unavailable (M_{orate} is the rate of seismic moment release on the fault, equal to μAS , in which μ = the rigidity modulus, 3×10^{11} dyne/cm², A =fault area, and S =fault slip rate in cm/yr). Where possible, we use the preferred values of D , S and T in equations 1 - 4, and otherwise use values that are the means of the minimum and maximum values. We also use the mean or preferred values of M_{max} (Appendix 1) in the equations.

Recent field studies and interpretations have resulted in major changes to estimated parameters of some of the fault sources since the Stirling et al. (1998) PSHA, and these require special explanation. These changes have occurred either for faults that have had alternative rupture segmentation models developed for them, or for faults or fault zones that have been mapped in more detail than before. Significant new field investigations have been carried out for the Alpine Fault (Berryman et al. 1998; Yetton et al., 1998), the Hope, Kakapo and Kelly Faults (Berryman & Villamor, unpublished field data), the Porters Pass Fault Zone and neighbouring faults (Pettinga et al. 1998; Stirling et al., 1999), and faults in the TVZ (Villamor & Berryman, unpublished field data). These new data have been incorporated into the PSH model. In the case of the Alpine Fault we develop southern (fault segment 5, in Fig. 2c) and two alternative northern (segment 6, Kaniere-Tophouse, and segment 8, Haupiri-Tophouse) rupture segments, and allow segments 5 and 6 to overlap in central Westland. This is in keeping with Yetton et al.'s (1998) explanation for the relatively short (c. 100-200 year) recurrence intervals for Alpine Fault earthquakes in central Westland. However, we also incorporate an alternative explanation for the short recurrence intervals, which is that the structural complexity of the central Westland area (i.e. where the Hope, Kelly and Kakapo Faults intersect the Alpine Fault) also allows shorter segments of the fault to rupture this section of the fault (Berryman pers. comm.). Specifically, we develop a 60km rupture segment (segment 7, Kaniere-Haupiri) that coincides with the overlap zone of the southern and northern segments. Recurrence intervals for all of the segments are then calculated with the constraint that they sum to the recurrence intervals derived from the field data. Over the 60 km long overlap zone, the combined recurrence interval is 200 years. For the Hope, Kelly and Kakapo Faults, the main difference in the treatment of these faults from Stirling et al. (1998) is that the southwestern extent of the Hope Fault (i.e. southwest of the Hammer Basin) has a considerably slower slip rate than previously assumed, and the slip rate surplus is instead taken up on the Kelly and Kakapo Faults (Berryman and Villamor pers. comm.).

For the Porters Pass Fault zone (Porters Pass, Coopers, Glentui, Lees Valley, Mt Thomas, and Mt Grey faults; Pettinga et al. 1998), we accommodate two equally plausible models for earthquake occurrence into the PSHA. These are a segmented



model, in which all six faults rupture as separate earthquake sources, and an unsegmented model, in which the whole fault zone ruptures in a single earthquake. Using eqs (1) to (4), the recurrence intervals of earthquakes for the two segmentation models are calculated by assuming that each model contributes to 50% of the slip rate along the fault zone.

Major improvements have been made to the fault database in the TVZ over that of Stirling et al. (1998). While the literature available to Stirling et al. (1998) only allowed them to incorporate 15 TVZ faults into the model, we now have a total of 54 TVZ faults in our model. The biggest improvement to the TVZ is the removal of the simplistic “Taupo Fault Belt North” and “South” sources (Stirling et al. 1998) and replacement with faults sources defined for that area in recent studies (Villamor pers comm).

We characterise the earthquake potential of the Hikurangi and Fiordland subduction zones in the virtual absence of any large-to-great earthquakes having occurred on the subduction interfaces in historic time, and a lack of paleoseismic data that can be attributed to subduction zone earthquakes. Our approach for the Hikurangi subduction zone is to combine the results of several alternative subduction earthquake models (Appendix 1). Two of these models (models 1 and 2) use empirical regressions developed from global subduction zone earthquakes (Abe, 1975; Somerville et al., 1999) to estimate the M_{\max} for earthquakes on the Hikurangi subduction interface from estimates of the area of subduction interface segments. The segments are defined from the results of Reyners (1998, 1999), and from changes in the cumulative slip rate of dip slip faults along the upper plate of the subduction zone in central Hawkes Bay (Beanland et al., 1998). The recurrence intervals for the subduction interface earthquakes are then estimated by taking account of the relative plate motion rates orthogonal to the subduction zone at the latitude of each segment, the amount of the plate motion taken up by dip-slip faults in the upper plate, and estimates of the degree of coupling (ratio of seismic slip to total slip) on the plate interface. The global average for the “coupling coefficient” is about 0.5 (Hyndman et al. 1997). Typical M_{\max} values of 7.5 to 7.9, (associated with single event displacements of about 3m) and recurrence intervals of between 140 and 400 years are estimated by way of models 1 and 2 if it is assumed that these earthquakes accommodate all of the coseismic slip on the interface. A third model (model 3) allows for the possibility that subduction zone earthquakes are great ($M > 8$), and therefore have much longer recurrence intervals (600 to 1200 years) if these earthquakes are assumed to accommodate all of the coseismic slip on the interface. The justification for model 3 is that earthquakes in the upper plate have produced large (~8m) displacements (e.g. 1931 M_w 7.8 Hawkes Bay earthquake), and these would be consistent with the stress regime of a strongly coupled subduction interface that slips with large single-event displacements (Haines & Darby, 1987). Furthermore, the short recurrence intervals



calculated for models 1 and 2 are in conflict with the absence of large subduction interface earthquakes in the historical record. If models 1 and 2 are entirely viable then we would expect there to have been at least one of these earthquakes on the five Hikurangi subduction interface segments in the last 150 years. In Appendix 1 we combine the three models to develop a subduction interface earthquake model with a weighting scheme that gives model 3 a weight equal to the combined weights of models 1 and 2. The resulting recurrence intervals range from 600 to 2400 years for large to great Hikurangi subduction interface earthquakes.

For the Fiordland subduction zone, we use a relatively simple kinematic model that is based upon field observations, and is partially constrained by the relative plate motion. The Alpine Fault intersects the coast at Milford Sound, where it is known to have a displacement rate of 26 ± 6 mm/yr and is thought to fail in great earthquakes about every 300 years (Cooper & Norris, 1990; Sutherland & Norris 1995). The offshore geometry of faults, including the extension of the Alpine Fault, is known from detailed swath mapping and seismic reflection data, but little is known about fault slip-rates or earthquake potential (e.g. Delteil et al., 1996; Melhuish et al. 1999; Barnes et al. 1999; Wood et al. 2000; and references therein). The onshore region has been geologically mapped (e.g. Bishop, 1986; Bishop et al., 1990; Turnbull & Uruksi, 1993; Turnbull & Uruksi, 1995; and references therein), but there is no relevant paleoseismic data, and only preliminary data concerning the location of active fault traces (Van Dissen, 1993; Turnbull & Uruksi, 1995; GNS, unpublished data; Otago University, unpublished data). The existence of known faults with young (<3 Ma), strongly deformed and uplifted marine sediments adjacent to them (e.g. Turnbull & Uruksi, 1995), combined with significant topography that is spatially correlated with geological structures, suggests the region currently has a moderate or high tectonic tempo. In addition, the deformation pattern of basement rocks suggests Fiordland has moved >100 km north in the last 30 m.y., suggesting a minimum average strike-slip displacement rate of 3 mm/yr on faults east of Fiordland (Sutherland, 1999). Although there are insufficient data to construct a robust set of fault sources for southwestern South Island, our sources developed for this report are based on a wide range geological data.

We define offshore faults in this study on the basis of detailed bathymetric and seismic data that were collected by GNS, NIWA, and their predecessors during the last 30 years. There has been considerable collaborative GNS-NIWA effort during the last decade, and significant progress has been made towards mapping the location of offshore fault traces, and estimating their slip-rates. The estimation of recurrence intervals and maximum magnitudes is difficult for offshore earthquake sources, but is necessary and will require further collaborative effort.



3.2.2 Distributed Earthquake Sources

In addition to defining the locations, magnitudes and frequencies of large ($M_{7-7.9}$) to great ($M_{\geq 8}$) earthquakes on the crustal faults and subduction zones, we also allow for the occurrence of moderate-to-large ($M_{\sim 5}$ up to some maximum cutoff magnitude) “distributed” earthquakes both on and away from the major faults. Our main reason for considering distributed earthquakes in our PSHA is that a large percentage of earthquakes in the historical record have not occurred directly on the mapped faults. Of the 85 largest historical New Zealand earthquakes studied by Dowrick & Rhoades (1999) for modelling attenuation of intensity, only five ruptured the onshore land surface. Presumably the seismogenic width greatly exceeds the width of earthquake rupture in most cases, which allows the earthquakes to occur without rupturing the ground surface, either on mapped faults or on unknown faults. Such is the case for most earthquakes of less than $M_{6.5}$ in California (Wesnousky 1986). In New Zealand, a good example of a distributed earthquake is the M_w 6.8 1994 Arthur’s Pass earthquake, which occurred on a previously unknown fault, and did not rupture to the surface.

We apply a methodology developed from that of Stirling et al. (1998) to characterise the PSH from distributed earthquakes. We use the spatial distribution of seismicity recorded since 1840 to estimate the likely locations and recurrence rates of distributed earthquakes at a gridwork of point sources across and beneath the country. Our minimum magnitude for distributed earthquakes ($M_{5.25}$) is slightly larger than the $M_{5.0}$ typically used in PSHA (the lower-bound magnitude for damaging ground motions), and is chosen to eliminate the erroneously high short period accelerations predicted for $M < 5.25$ earthquakes with the McVerry attenuation model (Section 3.2). $M_{5.25}$ was also used as the minimum magnitude by Matuschka et al (1985).

We first divide the country into 37 seismotectonic zones (14 crustal and 23 deep zones enclosing the subsurface seismicity to a depth of 100 km; Fig 3). The zones are assigned depth ranges shown in Figure 3a for the crustal zones and in Figure 3b for the deep zones. For the purposes of this study, the bases of the crustal zones are assumed to correspond to the base of the seismogenic crust. The maximum cutoff magnitude (M_{cutoff}) is separately estimated for the 37 seismotectonic zones, based on criteria such as the approximate magnitude of the largest historical earthquakes that have not been able to be assigned to specific faults (e.g., the M_w 6.8 1994 Arthur’s Pass earthquake), how comprehensively the zone has been studied to identify active faults (i.e. the “completeness” of the fault database in that zone), and the particular tectonic regime of the zone (e.g. a zone likely to enclose blind thrusts). All zones are set at $M_{\text{cutoff}}=7.0$, except for zone 5 ($M_{\text{cutoff}}=7.5$; most of the zone is offshore, and few active fault studies have taken place onshore), zone 6 ($M_{\text{cutoff}}=7.8$; the zone has produced earthquakes up to this magnitude on blind thrusts), zone 8 ($M_{\text{cutoff}}=7.7$; the



zone has produced earthquakes close to this magnitude on previously unknown faults) and zone 14 ($M_{\text{cutoff}} = 7.1$, a magnitude slightly larger than the 1993 August 10 Fiordland earthquake).

The next step is to decluster the catalogue by the method of Reasenber (1985), and then use the method of McGinty (1999) to assign new depths to the "restricted depth" earthquakes. "Restricted depth" events are the large number of events in the catalogue that were randomly assigned depths of 5, 12 and 33km because of poor depth control. Our procedure is to then subdivide the catalogue according to the 14 crustal and 23 deep seismotectonic zones, with the seismicity in each zone shown in Figures 3a and 3b. We next define five layers of point sources over the map area (at depths of 10, 30, 50, 70, and 90km) with a spacing of 0.1° in latitude and longitude, and then use a Gutenberg-Richter distribution $\log N = A - bM_w$ (N =number of events \geq moment magnitude M_w , and A and b are empirical constants; Gutenberg & Richter, 1944) to estimate the recurrence rates of distributed earthquakes at each point source. Gutenberg and Richter found that this type of distribution of seismicity applied to large areas, and it has also been shown to describe the fault zone earthquakes that are less in size than the M_{max} of the fault (e.g., Stirling et al. 1996). The SEISRISK programme CALCRATE (Bender & Perkins, 1987; Hanson et al. 1992) is then used to calculate parameter b of the Gutenberg-Richter relationship for each seismotectonic zone, and that value of b is then assigned to each point source within the zone. CALCRATE allows the use of different magnitude completeness levels for various time periods to calculate parameter b , and is based on the methodology of Weichert (1980). Since the New Zealand historical earthquake catalogue is in general complete for $M \geq 4$ since 1964, $M \geq 5$ since about 1940, and $M \geq 6.5$ since 1840, we use these three completeness levels and time periods to calculate b for the zones. As with the b -values, the M_{cutoff} assigned to each point source is simply the M_{cutoff} of the enclosing seismotectonic zone.

Following calculation of the b -values, the earthquake hypocentres found inside each grid cell (i.e. within ± 10 km depth of the grid layer) are counted to give "N values" for each grid cell. Three N values are calculated for each grid cell based on the three generalised catalogue completeness levels and time periods in the earthquake catalogue; $N_1 = N(M \geq 4 \text{ for } 1964-97)$, $N_2 = N(M \geq 5 \text{ for } 1940-97)$, and $N_3 = N(M \geq 6.5 \text{ for } 1840-1997)$. Within each grid layer, the three sets of gridded N values, b and M_{cutoff} values are then spatially smoothed with a Gaussian smoothing function, following the methodology of Stirling et al. (1998). For each grid cell, the smoothing involves multiplying the N , b and M_{cutoff} values for the grid cell and all of the neighboring values within the particular grid layer (i.e., the values that are within a specified horizontal distance from the grid cell) by the Gaussian function, summing all of the products, and then dividing by the sum of all of the Gaussian functions. The equation is:



$$N \text{ or } B \text{ or } M_{\text{cutoff}}(\text{smoothed}) = \frac{\sum ((N \text{ or } B \text{ or } M_{\text{cutoff}}(\text{each site}))e^{-d^2/c^2})}{\sum (e^{-d^2/c^2})} \quad (5)$$

in which c is the correlation distance (50km), and d is the distance from the centre of the grid cell to the centre of each neighbouring grid cell (neighbouring grid cells greater than 3x the correlation distance from the grid cell are not used in equation 5). The Gaussian smoothing preserves the total number of earthquakes in the catalogue after every N value in the gridwork has been smoothed with equation 5. The 50km correlation distance is used since it has been found to produce a spatial distribution of N values that correlates well with the general seismicity patterns across the country (Stirling et al. 1998). No smoothing is done in the vertical axis (i.e. between the various grid layers). The recurrence rates of $M_{5.25} - M_{\text{cutoff}}$ events at each point source are then calculated from the three sets of smoothed N values by way of the following maximum likelihood method to give a Gutenberg-Richter A -value based on the entire catalogue:

$$A = \log[(N1 + N2 + N3)/(tb1 + tb2 + tb3)] \quad (6)$$

in which,

$$\begin{aligned} tb1 &= ctime1 \times 10^{(-magmin1 \times b)} \\ tb2 &= ctime2 \times 10^{(-magmin2 \times b)} \\ tb3 &= ctime3 \times 10^{(-magmin3 \times b)} \end{aligned}$$

and,

$$ctime1 = 1997-1964; \quad ctime2 = 1964-1940; \quad ctime3 = 1940-1840.$$

The A value is then used in the Gutenberg-Richter relationship (this time equal to $\log N/\text{yr} = A - bM$) to solve for $N/\text{yr}(M \geq 4)$, and then the incremental rates ($n/\text{yr} = M$) are calculated for each 0.1 increment of magnitude from $M_{5.25}$ to M_{cutoff} . We show plots of the b -value, $N/\text{yr}(M \geq 4)$ for the five depth layers, and M_{cutoff} for the 10km (crustal) layer in Figure 4. Since M_{cutoff} is set to 7 for all of the deeper zones, we do not show the M_{cutoff} for these zones.

Our methodology for the treatment of distributed seismicity is an improvement over the commonly used approach in PSHA of defining large area source zones over a region and uniformly distributing the seismicity recorded inside each source across the source. This is because our methodology preserves the smooth transitions in seismicity rates within and across the boundaries of the seismotectonic zones, and avoids the "edge effects" that often appear on hazard maps when adjacent area sources enclose areas of significantly different seismicity rates. Though Peek's (1980) use of "fuzzy" boundaries between area sources removed these "edge effects"



in early New Zealand PSH maps, our methodology also preserves spatial variations of seismicity *within* the sources. Our methodology is also an improvement over that of Stirling et al. (1998), who only considered crustal seismicity, a single completeness level ($M \geq 4$ for the period 1964-96), single M_{cutoff} (7.5), and single b value (1.1) for the entire country. In Figure 4 we show maps of the distribution of $N(M \geq 4)$ per year, the b -value and the M_{cutoff} for the various layers of point sources in our model. Note that M_{cutoff} is set to 7.0 for all except the 0 to 20 km depth layer. It has the disadvantage that for some grid points in low seismicity locations N1, N2 and N3 will be zero, because the seismicity rates are lower than can be detected in the observation periods, while the true seismicity is non-zero. The lowest seismicity rate that can be detected with 90% certainty in the 33 year completeness period for $M \geq 4$ from a 50km radius circle is approximately 8×10^{-4} events per year per $0.1^\circ \times 0.1^\circ$ grid cell.

3.3 Attenuation Model

3.3.1 Introduction

The attenuation relationships used in this study have been developed recently by McVerry et al. (2000) for 5% damped acceleration response spectra (SA(T)) from a data set of New Zealand earthquake records, supplemented by p_{ga} values from overseas records in the near-source range (less than 10km source-to-site distance) that is lacking in the New Zealand data. The attenuation model takes account of the different tectonic types of earthquakes in New Zealand (i.e. crustal, subduction interface and dipping slab) and their range of centroid depths. The attenuation expressions for crustal earthquakes have further subdivisions, through mechanism terms, for different types of fault rupture (strike-slip, normal, oblique/reverse and reverse). The model was developed for site classifications which were based on those of the current New Zealand Loadings Standard NZS4203:1992, with one modification of the site classifications to give better matching of the New Zealand spectra, and a subdivision of the rock classification for specialist applications. A term was also included in the attenuation expression to model the rapid attenuation of high-frequency motions through the Taupo Volcanic Zone.

The McVerry et al. attenuation model is used in this study because it has specific relevance to New Zealand conditions, in contrast to most other available attenuation relationships, which were developed from either global strong motion data or data from other regions of the world. The McVerry et al. model is presented below, including discussion of features that affect the hazard estimates calculated in this study. Graphs of the p_{gas} estimated from the attenuation model as a function of magnitude, distance, tectonic type and focal mechanism, are shown in Appendix 2, along with spectra for a selection of magnitudes, source-to-site distances and tectonic



types. All plots are for site class B, the class assumed for all results presented in this report.

3.3.2 Site Classification

The development of the response spectrum attenuation model began using the site class categories (a), (b) and (c) of the current New Zealand Loadings Standard NZS4203:1992 (Standards New Zealand, 1992). In NZS4203:1992, category (a) nominally corresponds to rock or very stiff soil sites with natural periods less than 0.25s, category (b) corresponds to intermediate soil sites and category (c) to flexible or deep soil sites with natural periods estimated as greater than 0.6s. The Standard gives thicknesses of various types of soil that conform to categories (a) and (c).

It was found that stiff soil sites included in the NZS4203 site category (a) “rock or very stiff soil” exhibited p_{gas} and spectra similar to the category (b) “intermediate soil sites” rather than to rock sites. Accordingly, category (a) sites with more than 3m of soil were combined with category (b) sites to form the new class B. This separation of the stiff soil sites of category (a) from rock sites was also found necessary in the development of the Zhao et al. (1997) p_{ga} attenuation model. NZS4203:1992 category (c) “flexible or deep soil sites” carried over directly to Class C. Classes B and C were combined into a single “soil” class for the Zhao et al. p_{ga} study, but the differences in the site terms were statistically significant at longer periods in the response spectrum study, and were retained for all periods.

Class B is defined as soil sites with periods less than 0.6s. If the shear-wave velocity profile is known for a site, NZS4203:1992 allows the period to be estimated from four times the shear-wave travel-time from rock to the surface. Measured velocities or travel-times are usually not available for New Zealand sites, so most site classifications are made from the descriptions of the materials at the sites and their thicknesses. Table 1 lists the depths of different types of materials given in the code as corresponding to the changeover between classes B and C, with lesser depths taken as class B.

The New Zealand site classifications are based on estimated or measured travel-times from “rock” to the surface, rather than on the average shear-wave velocity in the top 30m as in recent US building codes. The main differences between the New Zealand and US classifications arise where there are thick deposits of reasonably high-velocity materials, such as gravels, over rock. The New Zealand classification recognises that these sites have the potential of amplification at periods around their site periods, so does not include them in the same class as shallower deposits of the same materials which do not have the potential for substantial amplification at moderate-to-long periods.



The site classifications also differ from those of the Abrahamson & Silva (1997) and Youngs et al. (1997) attenuation models that served as the starting points for developing the New Zealand response spectrum attenuation expressions for crustal and subduction zone earthquakes respectively (see Section 3.3.3). Abrahamson & Silva (1997) combined rock sites and sites with shallow soil up to 20m thick in their “rock” class, which is thus intermediate between the New Zealand classes A and B. Their “soil” class consists of deep soil greater than 20m thick, similar to New Zealand class C but including some class B sites as well. The Youngs et al. (1997) rock class is similar to New Zealand Class A, but their soil class is for soil greater than 20m thickness, with shallow soil not covered by either of their classes. Both studies excluded soft soil with shear wave velocities less than 150m/s, as in the development of the McVerry et al. model.

Also relevant for comparing the results with earlier New Zealand hazard studies are the site classifications used by Katayama (1982). Katayama’s four ground types were as used for bridge design in Japan. Type I is Tertiary or older rock (bedrock), or a diluvial layer of less than 10m thickness above bedrock, with natural periods less than 0.2s. Type II is more than 10m of diluvium or less than 10m of alluvium, with site periods between 0.2s and 0.4s. Type III is an alluvial layer less than 25m thick, with less than 5m thickness of liquefiable or low-strength soil, with site periods between 0.4s and 0.6s. Type IV is other than the above, usually soft alluvial layers or reclaimed land, with site periods exceeding 0.6s. In Japanese design practice, Types II and III are usually combined. Categories (a), (b) and (c) of NZS4203:1992 were interpretations for New Zealand condition of Types I, II/III and IV respectively, so can be compared directly to the corresponding Katayama ground types.



**TABLE 1: DESCRIPTION OF SITE CLASS B CLASSIFICATION
BASED ON NZS4203:1992**

Site Class B (Intermediate soil sites)

Sites where the low amplitude natural period is less than 0.6s, or sites with depths of soils less than the following values:

Soil type and description		Depth of soil (m)
Cohesive soil	Representative undrained shear strengths (kPa)	
Soft	12.5-25	20
Firm	25-50	25
Stiff	50-100	40
Very stiff	100-200	60
Cohesionless soil	Representative SPT (N) values	
Loose	4-10	40
Medium dense	10-30	45
Dense	30-50	55
Very dense	> 50	60
Gravels	> 30	100

The code commentary notes that the soil descriptions and associated properties correspond to those of the New Zealand Geomechanics Society (1988), "Guidelines for the Field Description of Soils and Rocks in Engineering Use".

It also notes that:

"Where a site consists of layers of several types of material, the contribution of each layer to the natural period may be estimated by multiplying 0.6s by the ratio of its thickness to that listed for its soil type. The total period may then be estimated by summing the contribution for each layer."

3.3.3 Form of the McVerry et al. Model

Limited ranges of magnitude and distance and insufficient records in the response spectrum dataset prevented the development of a robust model purely from the New Zealand data. Instead, overseas attenuation models that provided reasonable matches to the New Zealand data were selected as "base models", and then some of their coefficients were modified to improve the matches. One base model was selected for



crustal earthquakes and another for subduction-zone earthquakes Constraints were imposed so that the selected models controlled the behaviour at short distances where New Zealand data were lacking.

As a starting point for the development of the McVerry et al. attenuation model, the New Zealand data were compared with recent overseas attenuation models by calculating residuals between the data for the various tectonic classes of earthquakes and the predictions of appropriate attenuation models. The Abrahamson and Silva (1997), Idriss (1991), Boore et al. (1997) and Sadigh et al. (1997) attenuation models were considered for crustal earthquakes, and the Crouse (1991) and Youngs et al. (1997) models for subduction zone earthquakes. The residuals were examined as a function of magnitude, distance, centroid depth and response spectrum period for each earthquake source and site category. All of the crustal models provided adequate fits to the New Zealand data at most periods. The two subduction zone models provided poor fits to New Zealand data from shallow slab and interface earthquakes, generally over-estimating the data at short spectral periods and under-estimating them at longer periods. As a result of these comparisons, the Abrahamson & Silva (1997) (A&S) model was selected as a suitable base model for crustal earthquakes, and the Youngs et al. (1997) model as the base model for subduction zone earthquakes.

The approach was to perturb the base models, constraining some parameters but modifying others to obtain better matches to the New Zealand data. The regressions for the free coefficients were performed using the Abrahamson and Youngs (1992) random effects methodology, using source code provided by Abrahamson. The random effects model is a maximum likelihood method that accounts for correlations in the data recorded in the same earthquake. This is achieved by modelling two error terms, an intra-event residual and an inter-event residual. The inter-event residual gives the average error for data from the same earthquake event. The intra-event residuals represent the remaining variability in errors between data from the same event. The implementation of the random effects model in the McVerry et al. study allowed magnitude-dependent intra-event standard errors but inter-event standard errors that were independent of magnitude. Both the intra-event and inter-event standard errors were functions of spectral period, with the regressions for each spectral period performed separately.

The form of the model for the median response spectrum values for site class B is given in equation 7 for crustal earthquakes and in equation 8 for subduction zone earthquakes. The coefficient values are listed in Table 2.

For crustal earthquakes:

$$\ln SA_B(T) = C_1(T) + C_{4AS} (M-6) + C_{3AS}(T) (8.5-M)^2 + C_5(T) \Gamma +$$



$$(\mathbf{C}_8(T) + C_{6AS} (M-6)) \ln (r^2 + C_{10AS}^2(T))^{1/2} + C_{46}(T) r_{VOL} + C_{32} CN + C_{33AS}(T) CR \quad (7)$$

with $CN = -1$ for normal mechanism crustal earthquakes, 0 otherwise

$CR = 0.5$ for reverse/oblique mechanisms, 1.0 for reverse mechanisms, 0 otherwise

For subduction zone earthquakes:

$$\ln SA_B(T) = \mathbf{C}_{11}(T) + (C_{12Y} + (C_{15}(T) - C_{17}(T)) C_{19Y}) (M-6) + C_{13Y}(T) (10-M)^3 +$$

$$C_{17}(T) \ln (r + C_{18Y} \exp(C_{19Y} M)) + C_{20}(T) H_C + C_{24}(T) SI + C_{46}(T) r_{VOL} (1 - DS) \quad (8)$$

with $SI = 1$ for subduction interface earthquakes, 0 otherwise

$DS = 1$ for deep slab earthquakes, 0 otherwise

and $C_{15}(T) = C_{17Y}(T)$, and $C_{12Y}(T)$ the Youngs et al. coefficient of the (M-6) term

M is moment magnitude, r is the shortest distance in km from the site to the fault rupture, and r_{VOL} is the length in km of the part of the source-to-site path that lies in the volcanic zone. Other parameters are the mechanism for crustal earthquakes, indicated by CN and CR ; the tectonic type for subduction zone earthquakes, indicated by SI and DS ; and the centroid depth H_C for subduction zone earthquakes. Earthquakes within the subducting slab are separated into shallow slab earthquakes at depths less than 50 km, for which the predominant mechanisms are normal or oblique, and deep slab earthquakes which usually have reverse or strike-slip focal mechanisms. The equations apply for moment magnitudes 5 to 7.5, and distances up to 400 km.

Coefficients that were fitted in the regressions are shown in bold. Parameters subscripted $_{AS}$ and $_Y$ were held to Abrahamson & Silva or Youngs et al. values, respectively. The model expressions give the median (50-percentile) value of $SA_B(T)$, the 5% damped acceleration response spectrum value (in units of "g") for the stronger of two arbitrarily orientated orthogonal horizontal components for site class B.

$SA_B(T)$ has a log-normal distribution with median values given by equations 7 and 8 and magnitude-dependent standard errors $\text{Sigma}_{total}(M,T)$ of $\ln SA_B(T)$ defined in terms of the parameters $\text{Sigma}_{M6}(T)$, $\text{Sigslope}(T)$ and $\text{Tau}(T)$, as given in equations 9a and 9b. The parameter values are listed in Table 2.

TABLE 2: COEFFICIENTS OF THE ATTENUATION MODEL P2MRF5AC FOR SITE CLASS B

Period	0.000	0.075	0.10	0.20	0.30	0.40	0.50	0.75	1.00	1.50	2.00	3.00	
1	0.59021	1.64284	2.08360	1.63354	0.97823	0.68110	0.74598	0.26915	0.20183	-0.39613	-0.68381	-1.19739	free
3	0.00000	0.03000	0.02800	-0.01380	-0.03600	-0.05180	-0.06350	-0.08620	-0.10200	-0.12000	-0.12000	-0.17260	fixed
4	-0.14400	-0.14400	-0.14400	-0.14400	-0.14400	-0.14400	-0.14400	-0.14400	-0.14400	-0.14400	-0.14400	-0.14400	fixed
5	-0.00967	0.01011	-0.00958	-0.01061	-0.01108	-0.01044	-0.00944	-0.00859	-0.00709	-0.00751	-0.00751	-0.00674	free
6	0.17000	0.17000	0.17000	0.17000	0.17000	0.17000	0.17000	0.17000	0.17000	0.17000	0.17000	0.17000	fixed
8	-0.65469	-0.89543	-0.96827	-0.73174	-0.51073	-0.46256	-0.51891	-0.50359	-0.60867	-0.53197	-0.53197	-0.51984	free
10	5.60000	5.58000	5.50000	5.10000	4.80000	4.52000	4.30000	3.90000	3.70000	3.55000	3.55000	3.50000	fixed
11	8.98560	9.43477	10.15544	11.42270	10.40980	9.63810	9.53207	8.25309	7.85831	7.49288	7.20520	5.63637	free
12	1.41400	1.41400	1.41400	1.41400	1.41400	1.41400	1.41400	1.41400	1.41400	1.41400	1.41400	1.41400	fixed
13	0.00000	0.00000	-0.00110	-0.00270	-0.00360	-0.00430	-0.00480	-0.00570	-0.00640	-0.00730	-0.00730	-0.00890	fixed
15	-2.55200	-2.70700	-2.65500	-2.52800	-2.45400	-2.40100	-2.36000	-2.28600	-2.23400	-2.16000	-2.16000	-2.03300	fixed
17	-2.56727	-2.62147	-2.68877	-2.78783	-2.55600	-2.44827	-2.48662	-2.34444	-2.35600	-2.36279	-2.36279	-2.10982	free
18	1.78180	1.78180	1.78180	1.78180	1.78180	1.78180	1.78180	1.78180	1.78180	1.78180	1.78180	1.78180	fixed
19	0.55400	0.55400	0.55400	0.55400	0.55400	0.55400	0.55400	0.55400	0.55400	0.55400	0.55400	0.55400	fixed
20	0.01550	0.001778	0.01668	0.01470	0.01206	0.01354	0.01215	0.01008	0.00874	0.0071	0.00716	-0.00337	fixed
24	-0.50962	-0.58245	-0.71566	-0.77265	-0.68932	-0.40172	-0.34432	-0.10891	-0.02921	-0.1188	-0.11882	-0.30130	free
32	0.20000	0.20000	0.20000	0.20000	0.20000	0.20000	0.20000	0.20000	0.20000	0.20000	0.20000	0.20000	fixed
33	0.26000	0.26000	0.26000	0.26000	0.19800	0.15400	0.11900	0.05700	0.01300	-0.0490	-0.04900	-0.15600	fixed
46	-0.03279	-0.03430	-0.03573	-0.03831	-0.03582	-0.03342	-0.03238	-0.02855	-0.02539	-0.0201	-0.02012	-0.01651	free
SigmaM6	0.4865	0.5281	0.5398	0.5703	0.5505	0.5627	0.5680	0.5562	0.5629	0.5394	0.5394	0.5701	
Sigslope	0.1261	0.0970	0.0673	0.0243	0.0861	-0.1405	0.1444	0.0932	-0.0749	-0.0056	-0.0056	0.0934	
Tau	0.2687	0.3217	0.3088	0.2726	0.2112	0.2005	0.1476	0.1794	0.2053	0.2411	0.2411	0.2406	
SigtotM6	0.5558	0.6184	0.6219	0.6321	0.5896	0.5973	0.5869	0.5844	0.5992	0.5909	0.5909	0.6188	

Model P2MRF5AC (T=2s adjusted)

Uses foreign data for PGA, with A and C overseas records repeated 5 times

Volcanic path term, two rock site classes, W and M/S,

Different attenuation coefficients for M/S and other classes, with r=0 constraints

PGA only data from PGA6F5AC.TXT, SA from QKE9_ALL.TXT r=0 crustal & SZ constraint, c28=0, c30=a11

SA'(T) coefficients from S2VPSMR model

Results generated 28/1-1/2/99, edited from *.OUT files 1/2/99 by G. McVerry, re-edited for class B only 29/3/00 distance 0-400km, c5*r term for crustal, common atten & depth term for SZ



$$\begin{aligned}
 \text{Sigma (M,T)} &= \text{SigmaM6(T)} + \text{Sigslope (T)} * (\text{M}-6) & 5 < \text{M} < 7 \\
 &= \text{SigmaM6(T)} - \text{Sigslope(T)} & \text{M} < 5 \\
 &= \text{SigmaM6(T)} + \text{Sigslope(T)} & \text{M} > 7
 \end{aligned} \tag{9a}$$

$$\text{Sigmatotal (M,T)} = \text{sqrt} (\text{Sigma(M,T)}^2 + \text{Tau(T)}^2) \quad \text{for all M} \tag{9b}$$

The McVerry attenuation model was derived from all the available New Zealand strong-motion data that satisfied various selection criteria, and also from some digital seismograph records converted to accelerograms to increase the number of rock records available. The New Zealand dataset lacks records in the near-source region, at distances of less than 11km from the source, and at magnitudes of M_w 7.3 and greater. Accordingly, some constraints have been applied to the attenuation models for the near-source regions, and for large magnitudes. In addition, for p_{gas} (i.e. SA(0s), the New Zealand records were supplemented with 66 overseas records at distances of 10 km or less from the source, which were included directly in the regression analysis for determining the model. The selection of near-source records included some from the Northridge and Kobe earthquakes. The near-source selection is representative rather than comprehensive. Some records were excluded because we had insufficient information about the source regions to define the shortest source-to-site distance or about site conditions to assign the appropriate New Zealand classification.

The near-source constraint used in the McVerry et al. study was to require that the crustal and subduction zone expressions for rock sites matched the magnitude-dependence of the base models at zero distance ($r=0$). The values of two of the coefficients, $C_4(T)$ and $C_6(T)$, of the crustal model governed by the near-source constraint differed insignificantly from their A&S values, so they were left unchanged. The constraint required that the quadratic magnitude term be as for A&S, i.e. $C_3(T)=C_{3AS}(T)$. For subduction zone earthquakes, the $r=0$ constraint led to a relationship shown in equation 8 for the coefficient of the $(M-6)$ linking the coefficients of the linear magnitude and $\ln(\text{distance})$ terms, and the cubic magnitude term had to be the same as in the Youngs et al. model. Also, coefficients that occurred nonlinearly in the attenuation equations were constrained to their values in the base models.

In common with many but not all modern attenuation relations, the attenuation expressions of equations 7 and 8 exhibit partial magnitude saturation at short distances, that is, there is less dependence on magnitude at short distances than at large distances. In the crustal earthquake expression, this is achieved through the $M \ln(\text{distance})$ term, as in the A&S model. For the subduction zone expression, it is achieved by adding the Youngs et al. magnitude-dependent expression to the distance in the $\ln(\text{distance})$ term.



A departure from the A&S model is that A&S had different values for the magnitude coefficient C_4 for the magnitude ranges less than and greater than magnitude 6.4. The coefficient was larger for the small magnitude range, leading to lesser magnitude saturation at magnitudes less than 6.4. In the regression against New Zealand data, it was found that using the large magnitude coefficient for all magnitudes gave a better fit. A consequence of this is that small magnitudes may have relatively stronger effects at short distances for the McVerry et al. model than for the A&S model. This modification to the model was introduced before the overseas near-source pga was introduced to the dataset used in the regressions, so that there were no data from distances less than 11km when this modification was introduced. This change is likely to be a factor in the observation that uniform hazard spectra estimated with the McVerry et al. model appear very sensitive to the lower cutoff magnitude, showing very strong shorter period components when magnitudes less than 5.25 are retained.

Another change from the A&S model was the introduction of the anelastic attenuation term $C_5(T)r$. This term was found necessary when the maximum distance range of the data was extended to 400 km, compared to less than 250 km in the A&S dataset. The increased distance range was used to obtain sufficient rock records and volcanic path records. In earlier forms of the model where the maximum distance for crustal data was restricted to 200 km, this term was statistically insignificant. The numerical value of this term is small for distances of a few tens of kilometres or less that govern hazard estimates for all but possibly the largest spectral periods considered in the model, but its inclusion affects the values of the coefficients $C_8(T)$ of the $\ln(\text{distance})$ terms.

High attenuation of earthquake waves in part of the volcanic region of the North Island has been recognised for many years (e.g. Haines, 1981). The increased attenuation in the volcanic region has been modelled by the term $C_{46}(T) r_{VOL}$ applied for crustal, shallow-slab and interface earthquakes, where the source-to-site path includes a distance r_{VOL} (km) through the whole TVZ. The determination of the whole TVZ as the highly attenuating region is described by Cousins et al. (1999). While the geometric attenuation term dominates for nonvolcanic paths at distances less than 100-200 km, the anelastic attenuation is of similar importance for volcanic paths for short spectral periods. For example, the total anelastic term halves pga values over only 16 km in the volcanic region, while requiring more than 70 km to have the same effect on its own (i.e. neglecting the geometric attenuation) outside the volcanic zone. The volcanic path effect is less severe for periods exceeding 0.5s.

For the purposes of this study, the whole TVZ was approximated by source zone 3 (Fig. 3a). As further approximations, the volcanic region attenuation term was applied to the whole path for sources (both distributed point sources and fault sources) within zone 3, but ignored for the part of the travel path through zone 3 of earthquake waves propagating from sources outside it.



Similar effects to the volcanic region attenuation occur at depth (e.g. Mooney, 1970), but were ignored in the McVerry et al. study for deep-slab earthquakes because of the difficulties of modelling the high attenuation zone in three dimensions. Deep-slab records likely to have been affected by high attenuation in the mantle under the volcanic region were omitted from the analysis.

The model will significantly over-estimate the spectra from deep-slab sources involving propagation through the highly attenuating mantle. Work is in progress identifying the source and site combinations affected by high attenuation in the mantle, and developing a volcanic-path type modification to the attenuation expression of equation 8 for highly-attenuating mantle paths.

For crustal earthquakes, there are mechanism terms, C_{32} CN for normal-mechanism earthquakes and $C_{33AS}(T)$ CR for reverse/oblique or reverse mechanisms. Both of these terms were constrained in the analysis, the reverse/oblique term to period-dependent large-magnitude values from A&S model, and the normal term to a constant value based on analyses by Spudich and Abrahamson (Abrahamson, pers. comm.). The normal mechanism term corresponds to a factor of 0.82 on strike-slip spectra accelerations for all periods, and the reverse mechanism term to factors on the strike-slip accelerations varying from 1.30 in the 0s to 0.2s range, to 1.01 at 1s period, and 0.86 at 3s period. A&S had larger reverse-mechanism factors at magnitudes less than 6.4, with a maximum short-period factor of 1.84 for magnitudes of 5.8 and less, but such strong magnitude-dependence of the reverse-mechanism term was not supported by the New Zealand data.

The subduction zone expression for weak rock is based on the rock expression of Youngs et al. (1997). The coefficient $C_{17}(T)$ of the $\ln(\text{distance})$ attenuation term has been fitted from the regression against New Zealand data, but subject to the constraint that the magnitude dependence at zero distance is the same as for the Youngs et al. model. Period-dependent coefficients of the interface and centroid depth terms were fitted from the regression analysis, rather than taken as the constant values of the Youngs et al. model which were fitted from pga data but applied for all spectral periods. In the McVerry et al. model, the period-dependent interface coefficients show much stronger slab motions relative to interface motions than for the Youngs et al. model in the 0.1s to 0.3s range, and lesser slab versus interface effects for periods of 0.4s and greater. The interface coefficients correspond to ratios close to 1.0 for periods of 0.75s and greater. The depth effect is much greater than for the Youngs et al. model, especially for periods up to 1s.

Separate additive terms with respect to shallow-slab earthquakes were considered for interface earthquakes and deep-slab earthquakes, but were statistically significant only for interface earthquakes, as in the Youngs et al. model. Differences in attenuation rates



for shallow-slab, deep-slab and interface earthquakes were not statistically significant. Consequently, modelled spectral accelerations for shallow- and deep-slab earthquakes differ only by the effect of the depth term, and by the inclusion of the volcanic path term for shallow-slab earthquakes.

The Youngs et al. model gave nonlinear site effect terms through having different coefficient values in the rock and soil attenuation expressions. In the McVerry et al. model, site effects for soil sites were modelled directly through site response terms, with the same site effect terms imposed for crustal and subduction zone earthquakes. Nonlinear soil response factors that are a function of the estimated median weak-rock $pgas$, as used by A&S, were allowed to model the ratios of the spectra for soil sites, classes B and C, with respect to those for weak-rock sites. However, a linear site response factor was found to give the best fit for site class B, although this result may reflect the paucity of records of strong near-source motions for which any nonlinear effects would be most apparent. Nonlinear soil response factors were retained for Class C sites (not presented in this report), for which the modelled spectra are amplified with respect to those for weak-rock sites at short periods at low amplitudes of motion, but deamplified for strong motions. The site response factor for Class B has been included in the constant terms $C_1(T)$ for crustal earthquakes and $C_{11}(T)$ for subduction zone earthquakes in equations 7 and 8.

There were fewer response spectra than pga records available for the study, because (a) acceleroscope and undigitized records contribute $pgas$ but no spectra; (b) response spectra data were included only for frequencies where their amplitudes exceeded noise levels; and (c) near-source overseas records have been used only for $pgas$ to date. It was found that the pga estimates $SA'(0)$ from the response spectrum dataset were different from the estimates $SA'(0)$ from the larger pga dataset. The differences were most important for near-source $pgas$ from crustal earthquakes on rock and deep soil sites. The estimates were more in line with overseas models for the pga than for the response spectrum dataset, with the $SA'(0)$ values generally less than those from overseas models. It was decided to scale the response spectrum values for other spectral periods by the pga ratio, thus retaining the spectral shapes from the response spectrum dataset. This modification is incorporated in the coefficients listed in Table 2. This approach has the potential problem of imposing inappropriate spectral shapes near-source if the near-source spectral shapes $SA(T)/SA(0)$ are in fact different from those at greater distances. It is intended to include near-source overseas spectra rather than just pga values in future development of the attenuation model, in that we now have most of the spectra as well as pga values available.



3.4 Computation of Hazard

We use the locations, sizes, tectonic types or crustal mechanisms (slip types), and recurrence rates of earthquakes defined in our source model to estimate the PSH for a gridwork of sites with a grid spacing of 0.1 degrees in latitude and longitude (about 10km spacing). Our measures of PSH are the acceleration levels (pga, 5% damped response spectral acceleration at 0.2 and 1s period) with 475 year and 1000 year return periods at class B (intermediate soil) sites. We use the standard methodology of PSHA (Cornell, 1968) to construct PSH maps. For a given site, we: (1) calculate the annual frequencies of exceedance for a suite of ground motion levels (i.e. develop a "hazard curve") from the magnitude, recurrence rate, earthquake type, and source-to-site distance of earthquakes predicted from the source model; and (2) estimate the maximum acceleration level that is expected with a 10% probability of exceedance in 50 and 105 years. These time periods and probabilities are chosen to show the accelerations that have return periods of 475 and 1000 years, respectively. These are return periods of interest to engineers and planners. For each site, step (1) is repeated for all sources in the source model, and (2) is calculated by summing the results of (1) to give the annual frequencies of exceedance for a suite of acceleration levels at the site due to all sources (i.e. acceleration levels of 0.05g, 0.1 to 2g at increments of 0.1, and 3g), and finding the ground motion levels that correspond to annual frequencies of 1/475 and 1/1000.

In calculating the ground motions expected in a certain time period, we assume a Poisson model of earthquake occurrence, in that we base our estimates of hazard on the average time-independent rate of earthquake occurrence on each fault, and do not calculate time-dependent hazard that would take into account the elapsed time since the last earthquake on the fault. The Poissonian model is also applied to the Alpine Fault, in contrast to the methodology used in our recent PSHA for the Canterbury region (Stirling et al. 1999) which considered time dependent estimates of earthquake probabilities for the Alpine Fault (Yetton et al. 1998). We treat the Alpine fault in this manner since there is currently active debate going on as to the most appropriate conditional probability model for assessing earthquake probabilities (e.g. Ellsworth, 1999). In our calculation of ground motions with the McVerry attenuation model we adopt the standard practice of modern PSHA and take into account the uncertainty in estimates of ground motion from the attenuation model in the calculation of PSH. The general method is to assume that each estimate of ground motion calculated with the attenuation equation at a site is the median of a log-normal distribution, with an associated standard deviation. The standard deviations are usually equal to about 0.5 in natural log units of ground motion. The median and standard deviation are then used to estimate the probability of exceedance for a suite of ground motion levels up to 3 standard deviations below and above the median. Only magnitudes 5.25 and greater are included in the hazard analysis as discussed in Section 3.2.2.



Since the McVerry attenuation model has separate expressions for crustal earthquakes of different slip type or focal mechanism (i.e. strike slip, normal and reverse, and slip types intermediate between these extremes), and separate expressions for subduction interface, shallow slab and deep slab earthquakes, we estimate accelerations with the attenuation expression applicable to the slip type and tectonic environment of each earthquake source. Each fault is assigned a particular slip type, and the attenuation expression for that slip type is used for the fault in the hazard calculations. In the case of the dipping subduction interface sources we use the interface attenuation expression. For the distributed seismicity (point) sources, the slip type assigned to the point source is the slip type of the enclosing seismotectonic zone (Fig. 4). For the deep zones we simply use the shallow and deep slab expressions, based on the observation that essentially all of the deep seismicity in the country is attributed to the dipping Hikurangi and Fiordland slabs. Application of the “volcanic path” attenuation expression for the TVZ, which strongly reduces accelerations with distance, is limited to faults and point sources located in the TVZ, taken as corresponding to seismotectonic zone 3 of Fig. 3a. More sophisticated application of the “volcanic path” term (e.g. attenuation of accelerations passing through the TVZ from outside sources) cannot be performed until the 3-dimensional geometry of the TVZ is better defined. The deep slab expression is valid only for source-to-site paths up the dipping slab. We use it for all sites for deep slab sources, overestimating the motions for those sites involving propagation paths through the highly attenuating mantle.

3.5 Hazard Estimates

3.5.1 Hazard Maps

In Figure 5 we show maps of the levels of p_{ga} and 5% damped response spectral acceleration (0.2, and 1s period) with return periods of 475 and 1000 years (10% probability of exceedance in 50 and 105 years, respectively). Incorporation of fault data into the PSH model produces very different patterns of hazard across the region to the earlier maps of Matushka et al. (1985) and Smith and Berryman (1983, 1986), and generally similar patterns of hazard to the maps of Stirling et al. (1998). The highest 475 year accelerations (p_{gas} of over 1g, 0.2s spectral accelerations of over 3g, and 1s accelerations of over 0.6g) occur in the west of the South Island. These areas are in the vicinity of the Alpine, Hope, Kakapo and Kelly Faults (fault segments 5, 7 and 150-152 in Fig. 2). The latter three faults are also in areas of relatively high distributed crustal seismicity. Relatively high 475 year accelerations at short spectral periods (peak accelerations of <0.6g outside the Alpine Fault high hazard zone for 475 years) 0.5g, and 0.2s spectral accelerations of over 1.4g) are also observed in north Westland and western Nelson, and these are attributed to the high distributed



seismicity rates in the area of the Buller and Inangahua earthquakes. However, since these distributed seismicity sources produce many more moderate earthquakes than large earthquakes, the long period (1s) accelerations only amount to 0.2 to 0.3g.

The highest accelerations in the North Island occur along the northeast striking faults of the Axial Tectonic Belt and TVZ. Here, pga and 0.2s and 1s spectral accelerations reach maximum values of over 0.6g, 1.8g, and 0.5g, respectively over small areas. The TVZ faults and distributed seismicity source also produce a zone of high hazard to the southwest and northeast of Lake Taupo on the 475 year maps. The contribution to the 475 year hazard from the Hikurangi subduction zone is to produce a broad zone of relatively high hazard from the TVZ to the East Coast. For pga this measures about 0.3 to 0.4g, and the corresponding values of 0.2s spectral acceleration are 1.2 to 1.4g, and 0.2 to 0.4g for 1s acceleration. Hazard progressively decreases to the south and north of all of these areas. The lowest hazard in the country is in Northland, and the lowest in the South Island is in Southland (Fig. 6). The hazard may be underestimated in these regions, in that the seismicity rate has been modelled as zero in places, while the minimum rate of earthquakes that can be detected with 90% reliability from the completeness levels of the historical seismicity catalogue is approximately 8×10^{-4} events per year greater than magnitude 4 per $0.1^\circ \times 0.1^\circ$ grid cell.

The 1000 year PSH maps generally show much higher hazard than the 475 year maps, for the simple reason that the longer timespan allows more earthquakes to contribute to the hazard. All of the areas described above show highest hazard on the 1000 year maps. Differences of 0.1g for pga and 1s spectral acceleration, and 0.2g for 0.2s spectral acceleration are typically observed between the maps. Some of the largest differences in pga (differences of 0.2g) are observed in the foothills of the Southern Alps, northwest of Christchurch.

The PSH maps generally show a smooth distribution of hazard that is highest along the major plate boundary faults of the axial tectonic belt and the subduction zones, and progressively decreases away from these areas. However, this progressive decrease in hazard is locally interrupted by zones of anomalously high or low hazard. A small circular zone of unusually high hazard appears on most of the maps in northern Southland/southern Central Otago. This zone is attributed to the relatively short earthquake recurrence intervals estimated for the Blue Mountain and Spylaw Faults (Appendix 1, faults 162 and 163 on Fig. 2). Since these recurrence intervals are simply based on field reconnaissance of the area, and not detailed field investigations (Stirling et al. 1998), the hazard in this zone may be unrealistically high. Another area of anomalous hazard is in the TVZ, to the south of Lake Taupo. This area does not show as high hazard as the area north of Lake Taupo, yet the extension rate across the TVZ is presumed to be similar in all areas. The discrepancy may be due to incomplete knowledge of the TVZ faults south of Lake Taupo. The small zones of



high hazard in the Raukumara Peninsula region (area of Gisborne, East Cape and the northeastern Bay of Plenty) are attributed to faults characterised from field reconnaissance (Mazengarb pers comm.). Since the area has not been the focus of detailed paleoseismic investigations, two possible explanations for the small zones of anomalously high hazard are: (1) that there may be many more, as yet undiscovered active faults in this area that would homogenise the hazard if incorporated into the model, and; (2) that earthquake recurrence intervals for the faults in the area have been underestimated, leading to overestimation of the hazard at sites close to these faults. Lastly, the “corridor” of lower hazard between Rotorua and Mount Maunganui on the 475 year pga map is due two factors. The first is the effect of the Kerepehi Fault (fault segments 94-97 in Fig. 2a) to the northwest of TVZ adding to the hazard from the distributed seismicity. The second is the use of the “volcanic path” attenuation expression for distributed earthquake sources in the TVZ (seismotectonic zone 3 in Fig. 3), which reduces the 475 year pga in the corridor from that to the northwest for this part of the TVZ that has no modelled fault sources (Fig. 2a).

There are some notable differences in the PSH maps produced in this study from those of Stirling et al. (1998), despite the generally similar pattern of hazard across the country as a whole. Some of the largest differences are located in the Raukumara peninsula area, and are attributed to differences in modelling of the Hikurangi subduction interface in the two studies. The Stirling et al. study assumed an uncoupled Hikurangi subduction zone in this area (i.e. nil potential for subduction interface earthquakes), which resulted in much lower hazard than the hazard shown in Figure 5. The other large difference is that the hazard is lower than estimated by Stirling et al. in the TVZ. This is due to the major differences in modelling of the TVZ faults in the two studies, and implementation of the volcanic path attenuation relationship in our study.

3.5.2 Site Specific Hazard

In addition to defining maps of the expected levels of pga and spectral accelerations for New Zealand, we also compare the PSH model at five sites from diverse seismotectonic environments around the country. The sites are the four major populations centres (Auckland, Wellington, Christchurch, and Dunedin), which respectively come from areas of low, high, low and low concentrations of active faults and historical seismicity, and Otira, located in the area of highest hazard in the country (Fig. 5).

In Figure 6 we show hazard curves (graphs of the annual rate of exceedance for a suite of acceleration levels) for the five centres. The annual rate of exceedance is the inverse of the return period. There is considerable spread in the graphs of pga (Fig. 6A) and 1s response spectral acceleration (Fig. 6B) for the five centres. Specifically,



the graphs show more than a factor-of-10 to 100 range in annual rate for a given acceleration, and about a factor-of-10 range in acceleration for a given annual rate. Clearly the township of Otira shows the highest hazard, consistent with a location close to major active faults (e.g. Alpine Fault), and within an area of relatively high historical seismicity (Fig. 3). In decreasing order of hazard are the centres of Wellington (close to five major faults, above the Hikurangi subduction interface, and in an area of high historical seismicity), Christchurch (at a distance of about 50km from a number of active faults in the foothills of the Southern Alps), and Dunedin and Auckland (both generally away from areas of active faults, and in areas of relatively low seismicity rates). The slopes of the hazard curves are generally similar, except for the lower-than-average slopes for pga in Dunedin and Otira (Fig. 6A), and the higher-than-average slopes at long return periods (>500 years) for Otira. The increasing influence of the Akatore Fault on the hazard for Dunedin as the return period increases takes Dunedin from hazard levels similar to those of Auckland at return periods of about 100 years and less up to levels similar to those of Christchurch at return periods of several thousand years. For Otira, the short average recurrence intervals of rupture on neighbouring active faults that govern its hazard lead to saturation effects becoming apparent for return periods exceeding about 500 years.

The five centres can also be compared by way of response spectra calculated for given return periods. In Figure 7 we show spectra for return times of 475 years (i.e. 10% probability of exceedance in 50 years; Fig. 7A) and 1000 years (Fig. 7b). The spectra for all five centres show their highest accelerations at the 0.2s spectral level (a typical observation in strong motion seismology), and the pgas are slightly greater than the 1s spectral acceleration for all spectra. The 1000 year spectrum generally shows around a one-third increase in accelerations over the 475 year spectrum for a given centre, except for Otira where the increase is about 25% and Dunedin where it is around 50%.

Next, we show disaggregation plots for the five centres in Figure 8. These plots show the percentage contribution to the hazard for a particular return period from the various earthquake sources in the source model. They demonstrate the different contributions of magnitude and distance that govern the hazard in the five locations, and the different contributors to the hazard for short (e.g. pga) and long (e.g. 1s) spectral periods. In Figure 8 we show disaggregation plots for pga and 1s spectral acceleration, for 475 year and 1000 year return times. Twenty plots are shown in total.

In the case of Auckland, virtually all of the hazard comes from the distributed seismicity sources, which contribute over 97% of the pga hazard and about 85% of the SA(1s) hazard for the 475-year and 1000-year return periods considered. The Kerepehi North Fault (segment 94 in Fig 2a and Appendix I), modelled as producing



magnitude 6.7 earthquakes at a distance of 62km from Auckland with an average recurrence interval of 2500 years, makes a small contribution to the hazard in Auckland which is apparent in the SA(1s) disaggregation plots.

In contrast, Wellington's hazard is dominated by fault sources. The strong influence of the Wellington Fault is evident from the peaks on the disaggregation plots (Fig. 8) at Mw 7.3 and a distance of less than 10 km. The Wellington Fault, modelled with magnitude 7.3 earthquakes with an average recurrence interval of 600 years on the Wellington-Hutt Valley segment (Wellington SW, segment number 157) at a distance of 3 km, makes about a 60% contribution to the hazard of Wellington for the four cases considered. The second largest peak in the pga plots corresponds to the contribution (about 15%) from the Wairarapa Fault (segment 58) in magnitude 8.1 earthquakes at 20 km distance. The Wairarapa Fault makes a similar percentage contribution to the SA(1s) hazard, which also includes 10-15% contributions from the Hikurangi subduction interface (segments 63, 68 and 73) in the magnitude 7.8-8.4 range at about 23km distance under the city. Magnitude-distance cells corresponding to distributed seismicity sources rarely contribute more than 2% to the hazard (the small peaks at $M_w < 6$ and distance < 50 km) for return periods of 475 years and 1000 years.

The pga hazard of Christchurch comes from a combination of distributed seismicity sources at less than 50km (the peaks at $M_w < 6.5$ and distances < 50 km), contributing 55-60% of the 475-year and 1000-year hazard, and the faults at the western edge of the Canterbury Plains (e.g. Ashley Fault; the peaks at $M > 6.5$ and distances of 30km to 50km). The Alpine Fault (segment 5, Milford-Haupiri) only contributes a maximum of about 2% to the pga hazard of Christchurch, as seen in Figure 8 as the small peak centred at Mw 8 and a distance of 130km on the pga plots. On the other hand, the Alpine Fault is the single largest contributor to the SA(1s) hazard, at slightly over 20%. The other large peak in the SA(1s) disaggregation plots, centred at magnitude 7.2 and 30km distance, is the combined contribution of the Ashley, Springbank and Pegasus 1 Faults (segments 30, 31 and 32 in Fig. 2). The overall contribution from modelled faults is over 90% of the estimated SA(1s) hazard for Christchurch.

In Dunedin, most of the hazard comes from the distributed seismicity sources (the peaks at $M_w < 6.9$ and distances < 60 km) and from the Akatore Fault (fault 280), with magnitude 7.1 earthquakes at 13km distance with an average recurrence interval of 3000 years. The percentage contribution of the Akatore Fault to the 1000 year hazard (about 30% for both pga and SA(1s)) is about double the 475 year contribution of 16%. The distributed seismicity contributes 70-80% of the pga hazard and about 45% of the SA(1s) hazard for these return periods.



Lastly, the hazard at Otira is overwhelmingly dominated by large-magnitude earthquakes on the nearby faults that have short average recurrence intervals, with virtually negligible contribution to the hazard from the distributed seismicity sources. The Kelly Fault (fault 146) producing magnitude 7.2 earthquakes at a distance of about 2km from Otira contributes about 50% of the estimated pga hazard and 60-65% of the SA(1s) hazard for return periods of 475 years and 1000 years. The Milford-Haupiri segment of the Alpine Fault (segment 5) produces magnitude 8.1 earthquakes at a distance of about 10 km with an average recurrence interval of 300 years. The closeness of the fault sources and their associated large-magnitude earthquakes with short average recurrence intervals translate to very high estimates of the 475-year and 1000-year motions.

The last set of results presented (Figures 9a-e) are comparisons of the 475-year return period spectra for site class B at the five locations from this study (labelled 475 years NHM) with those resulting using the seismicity (Smith & Berryman) and attenuation (modified Katayama) models of the Matuschka et al. (1985) study. To separate the effects of changes to the seismicity and attenuation models between the current study and the 1985 study, results are also presented using the new seismicity model with the modified Katayama attenuation model used in 1985.

For Auckland, the new class B spectrum is typically about 80% of the 1985 values, although as low as about 50% at 1s period. At periods up to about 0.35s, the changes can be attributed about equally to the seismicity and attenuation components of the model. For periods of 0.4s and greater, the changes result almost totally from the attenuation model.

For Wellington, the short-period part of the spectrum (up to 0.5s) has increased considerably from that estimated from the 1985 model, especially around the peak of the spectrum at 0.2s period. The SA(0.2s) value has increased from 1.28g to 1.64g. This change appears to result almost entirely from the new attenuation model, in that the new and old (Smith & Berryman) seismicity models give very similar results using the modified Katayama attenuation model (results labelled “475yrs Matuschka” and “475yrs Mod. Katayama” respectively). However, this is misleading, in that the hazard disaggregations discussed previously (Figure 8) show that the 475 year hazard estimated for Wellington in the current study is dominated by contributions from fault sources. In particular, the Wellington-Hutt Valley segment of the Wellington Fault at a distance of 3km contributes about 60% of the estimated hazard. The Smith & Berryman seismicity model that was used in the 1985 study did not include fault sources, so the similarity of the results using the two different seismicity models with the modified Katayama attenuation model does not mean that the seismicity models are essentially the same around Wellington. The important feature is the combination of the new attenuation model with the new seismicity model. The modified Katayama



attenuation model is inappropriate for modelling near-fault motions, as it produces no change in estimated spectra for distances between 0km and 20km. The new McVerry et al. attenuation model produces a substantial increase in spectral accelerations as the distance decreases from 20km. It is thus able to produce estimates of the motions resulting from the Wellington Fault source (e.g. median pga of 0.60g and median SA(0.2s) value of 1.82g at 3km from a magnitude 7.3 strike-slip fault) that are much more in line with observed near-fault motions than the values (median pga= 0.26g, median SA(0.2s) = 0.66g) given by the modified Katayama model. At 0.75s and beyond, there is little difference in the results from the three models.

For Christchurch, the 475 year spectra are similar in character between the three models. The new model gives increased 475 year values with respect to the 1985 study up to 0.5s period, and similar values at longer periods. The results from the two seismicity models using the modified Katayama attenuation model are very similar. For Christchurch, estimation of near-source spectra accelerations is not a factor, so it appears that the seismicity distribution around Christchurch is approximately equivalent in the two seismicity models, although in the new model some of it is represented by fault sources at moderate and large distances rather than purely by distributed seismicity. The new attenuation model appears to give greater values than the modified Katayama model in the short-period range from 0.1s to 0.4s, and reduced values in the 0.75s-1.5s period band.

For Dunedin, the short-period spectral values from the new model are similar to those of the 1985 model, but reduced for periods of about 0.3s and greater. The comparisons using the modified Katayama model show a large decrease in spectral values for the new seismicity model. However, the much stronger motions associated with the Akatore Fault for the new attenuation model counteracts much of this difference.

For Otira, the new estimates are considerably increased because of the inclusion of fault sources. In the short-period band, the modified Katayama attenuation model is unable to produce the levels of near-source motion expected from the Kelly and Alpine Faults, so the new attenuation model boosts the estimated spectra considerably.

In summary, the new study produces considerably different results from the 1985 study. At some sites, particularly those near active faults, the estimated spectra have increased by large amounts, while at other locations the estimated spectra are reduced. The combination of a response spectrum attenuation expression that is able to produce realistic levels of near-fault motions with a seismicity model that includes fault sources is an important feature of the new seismic hazard model.



4.0 SUMMARY AND CONCLUSIONS

We have developed a new PSH model for New Zealand that incorporates geological data describing the location and earthquake recurrence behaviour of 305 active faults, a seismicity catalogue with greatly improved locations for many events, new attenuation relationships for pga and spectral acceleration developed specifically for New Zealand, and state-of-the-art PSH methodology developed in New Zealand and the USA. The model replaces the Matuschka et al. (1985) and Smith and Berryman (1986) models, which were largely based on the historical record of earthquakes. PSH maps produced from the new model show the highest hazard to occur in Fiordland (vicinity of the Fiordland subduction zone and the offshore extent of the Alpine Fault), along the axial tectonic belt (Westland, Marlborough, north Canterbury, Wellington, Wairarapa, western Hawkes Bay and eastern Bay of Plenty), the TVZ (from the central North Island volcanoes to the Bay of Plenty), and in the seismically active area of the Buller and Inangahua earthquakes (north Westland/southwest Nelson). As such, the maps show similar patterns of hazard to the experimental maps produced by Stirling et al. (1998), but considerably different patterns to those of Smith and Berryman (1983, 1986). Since the latter maps have long served as the basis for the loadings code, and have been applied to numerous engineering, planning, and insurance applications, our new maps are expected to produce significantly different estimates of hazard for future applications of this nature.

Interrogation of the PSHA at the four major centres reveals that they have the following rank in decreasing order of hazard: Wellington, Christchurch, Dunedin and Auckland. The hazard is highest in Wellington since it is close to a number of major active faults, and in an area of high seismicity in historical time. In comparison, the other centres are generally located in areas away from the major active faults, and in areas of relatively low seismicity rates. For Auckland, virtually all of the hazard comes from distributed seismicity sources. The disaggregation of the hazard shows a more complicated picture for Christchurch and Dunedin. For Christchurch, distributed sources contribute most of the pga hazard, but modelled fault sources contribute nearly all the hazard in terms of response spectral accelerations for 1s period. For Dunedin distributed seismicity sources are the most important at short return periods, but the Akatore Fault becomes increasingly important as the return period increases.



5.0 FUTURE DEVELOPMENTS AND SENSITIVITY STUDIES

We can identify a number of important areas of future research that will improve our estimates of seismic hazard for New Zealand. First, the estimates of PSH (Figs. 5 and 6) are provided for a single site condition (intermediate soils), and do not take into account the variable site conditions that exist across the country. Our attenuation model and computer code allows five site conditions to be modelled, with maps similar to Figure 5 able to be produced for each site condition. Variable site conditions may have a significant influence on ground motions in many areas of the country (e.g. low-lying areas of the Wellington region and areas of Christchurch). We therefore recommend that information on surface geology be factored into our PSHA to produce estimates of PSH that incorporate the actual site conditions at each location. At the simplest level this would involve choosing the site class applicable to the geology of each site (from published geological maps), and using the appropriate attenuation expression to estimate the PSH at that site. To more thoroughly address the issue of site conditions, basin effects should also be considered in future PSHAs. Research on this topic will eventually provide amplification factors due to basin geometry, and these will be readily imported into PSHA.

Another limitation of our study is that all the estimates of seismic hazard are made according to the preferred, or mean values of the various parameters (e.g. magnitude, recurrence rate, M_{cutoff} for distributed seismicity), and do not incorporate the uncertainties in these parameters. While it is standard practice for regional PSHA to use preferred parameters (as we have done), we recommend that the PSHA be extended to quantify the uncertainty in estimates of PSH as a result of our uncertainty in the input parameters. Such information will be most useful for the towns and cities, but could also be provided for the entire region. The most effective way of quantifying the uncertainty in input parameters is by way of a "Monte Carlo" style sampling of a logic tree analysis (Reiter 1991, pp. 220-222). Repeated sampling of a logic tree of parameters according to weights assigned to each choice of parameter (branch of the logic tree), calculation of the hazard with each sample of the logic tree, and comparison of all the hazard estimates will quantify the uncertainty in PSH. This is routinely achieved for site-specific PSHAs, but is uncommon in regional or national PSHAs.

For the distributed seismicity the historical catalogue includes a mix of magnitude scales. Conversion of these magnitudes to moment magnitude (M_w) involves considerable uncertainty, especially for deep earthquakes, that has not been taken into account in the present study. Rhoades (1996) has developed a methodology that accounts for these uncertainties in magnitudes that will be incorporated into the hazard calculations.



We have based our PSH estimates on time-independent (Poissonian) probabilities of earthquake occurrence, and have not taken into account the elapsed time since the last earthquake on any of the faults (conditional probability estimates). Effort should be focused on developing conditional probability estimates for the well studied faults in the country, such as the major strike-slip faults in the axial tectonic belt. One such model has been developed for the Alpine Fault (Yetton et al. 1998), but this model needs to be evaluated against alternative, equally plausible conditional probability models (e.g. Ellsworth, 1999). Also related to “non-poissonian” earthquake occurrence is the issue of fault interaction and earthquake clustering in space and time. Historical observations in areas like northern Turkey and the Central Nevada Seismic Belt (e.g. Caskey et al. 1997) provide evidence for earthquake clustering in space and time. In PSHA this information should be used to show that the probability of an earthquake on one fault is in part conditional on the occurrence of an earthquake on a neighbouring fault, and that the expected hazard of a region in one relatively short time period (e.g. 50 years) could be considerably different to the expected hazard in another such time period.

The parameters assigned to the Hikurangi and Fiordland subduction zones are entirely based on modelling, and are unconstrained by actual data. Increased effort needs to go into undertaking research to constrain the degree of coupling of the subduction interface, and the timing of large-to-great subduction interface earthquakes in the paleoearthquake record.

The attenuation model used in this study has some shortcomings that should be resolved. An example is the unusually high short-period accelerations produced by the model for $M < 5.25$ earthquakes. Future improvements to the strong motion database and further modelling of these data will undoubtedly improve the estimates of acceleration from the attenuation model, especially in the near-source zone. In addition, it is intended to incorporate other recent New Zealand attenuation relationship into the model, such as the Dowrick and Rhoades (1999) Modified Mercalli intensity expression, and the Zhao et al. (1997) pga model. For further analysis of the sensitivity of the results to the selection of the attenuation model, calculations will be performed for several overseas models. Currently the Abrahamson and Silva (1997), Sadigh et al. (1997), Katayama (1986) and modified Katayama (Matuschka et al. 1985) models are included in the computer code, to which the Boore et al. (1997) model will be added. Other future developments will be proper implementation of the TVZ attenuation expression, and modelling of the high attenuation in the mantle from deep slab earthquakes, as quantified for intensities by Dowrick and Rhoades (1999).

Finally, efforts should be focused on developing methods to test our estimates of PSH, and those of future PSHAs. Currently, many workers use historical earthquake records



to test PSH maps, but the short duration of historical records in most countries make them inadequate for testing PSH estimates that incorporate prehistoric earthquake data. Work on the use of field criteria such as precariously-balanced rocks to test the estimates of PSH is progressing in the western USA, and similar studies should be promoted in New Zealand. Precariously-balanced rocks may provide upper estimates of the ground motions that have occurred at specific sites for time periods of thousands of years (e.g. Stirling et al., 1998).



6.0 ACKNOWLEDGMENTS

The funding of the Earthquake Commission Research Foundation to produce this report is gratefully acknowledged. Numerous people in addition to those included as authors deserve acknowledgement for their assistance in this study. Martin Reyners and Terry Webb provided assistance in developing the earthquake recurrence intervals and magnitudes for the Hikurangi subduction zone. Julian Garcia collected much fault data from recent literature, and Colin Mazengarb provided assistance with developing fault parameters for the Raukumara peninsula. Jarg Pettinga and Mark Yetton provided many new data for this study via the Canterbury Regional Council seismic hazard analysis. Haidee Davidson and David Kennedy are thanked for report preparation. John Zhao, Norm Abrahamson, Paul Somerville and Nancy Smith contributed to the development of the New Zealand response spectrum attenuation relation, in studies partly funded by the former Electricity Corporation of New Zealand. Much of the work that has gone into developing the New Zealand model has been funded by the Public Good Science Fund.



7.0 REFERENCES

- Abe, K., 1975. Reliable estimation of the seismic moment of large earthquakes. *Journal of Physics of the Earth*, 23: 381-390.
- Abrahamson, N.A. and Youngs, R.R. 1992. A stable algorithm for regressions analysis using the random effects model. *Bulletin of the Seismological Society of America* 82: 505-510.
- Abrahamson, N.A. and Silva, W.J. 1997. Empirical response spectral relations for shallow crustal earthquakes. *Seismological Research letters*: 68, 94-127.
- Aki, K., and Richards, P.G. 1980. *Quantitative Seismology: Theory and Methods*, W.H. Freeman, San Francisco, California.
- Barnes, P., Davy, B., Sutherland, R., Delteil, J. 1999. Structure and kinematics of the offshore Fiordland margin, New Zealand. *Geological Society of New Zealand Miscellaneous Publication 107A*, p. 11.
- Beanland, S., Hancox, G. T., Townsend, T., Van Dissen, R. 1997. *Waikaremoana power station earthquake hazard assessment*. GNS client report 33397D.
- Beanland, S., Melhuish, A., Nicol, A., and Ravens, J. 1998. Structure and deformational history of the inner forearc region, Hikurangi subduction margin, New Zealand. *New Zealand Journal of Geology and Geophysics* 41: 325-342.
- Begg, J.G., and Van Dissen, R.J. 1998. Whitemans Valley Fault: a newly discovered active second order fault near Wellington, New Zealand – implications for regional seismic hazard. *New Zealand Journal of Geology and Geophysics* 41:441-448.
- Bender, B. and Perkins, D.M. 1987. *Seisrisk II: A computer program for seismic hazard estimation*. U.S. Geological Survey Bulletin 1772.
- Benson, A., Little, T., Van Dissen, R. J., Hill, N., Townsend, D., 1998. Paleoseismicity of the eastern section of the Awatere fault, New Zealand. *Programme & abstracts, Geological Society of New Zealand & New Zealand Geophysical Society Joint Annual Conference*. *Geological Society of New Zealand miscellaneous publication 101B* : 43.
- Berryman, K.R., and Beanland, S. 1988: The rate of tectonic movement in New Zealand from geological evidence. *Transactions of the Institute of Professional Engineers of New Zealand* 15: 25-35.
- Berryman, K.R., Beanland, S., Cooper, A.F., Cutten, H.N., Norris, R.J., Wood, P.R. 1992: The Alpine Fault, New Zealand: Variation in Quaternary structural style and geomorphic expression. *Annales Tectonicae Supplement to Volume 6*: 126-163.
- Berryman, K.R. , Hull, A.G, Smith, E.G.C. 1995. Deterministic estimates of earthquake hazard in Australasia: a comparison of Wellington, Auckland and Melbourne. *Pacific Conference of Earthquake Engineering*. *Australian Earthquake Engineering Society* 1 : 49-58.



- Berryman, K.R., Cooper, R.F., Norris, R.J., Sutherland, R., Villamor, P. 1998: Paleoseismic investigation of the Alpine Fault at Haast and Okuru. Geological Society of New Zealand and New Zealand Geophysical Society Joint Annual Conference. Programme and Abstracts. *Geological Society of New Zealand Miscellaneous Publication 101A*: 44.
- Berryman, K.R., Beanland, S., Wesnousky, S.G., 1998. Paleoseismicity of the Rotoitipakau Fault Zone, a complex normal fault in the Taupo Volcanic Zone New Zealand. *New Zealand Journal of Geology and Geophysics* 41 : 449-465.
- Bishop, D.G. 1986. *Geological map of New Zealand 1:50 000, Sheet B46-Puysegur, Map (1 sheet) and notes (36 p.)*, Dep. of Sci. and Ind. Res., Wellington.
- Bishop, D.G.; Blattner, P.; and Landis, C.A., 1990: *Miscellaneous map of New Zealand, Sheet 16 - Hollyford. Map (1:75 000) and notes (40 p.)*. Department of Scientific and Industrial Research, Wellington.
- Boore, D.M., Joyner, W.B., and Fumal, T. 1997: Equations for estimating horizontal response spectra and peak acceleration in western North American earthquakes. *Seismological Research Letters* 68 : 128-153.
- Caskey, S.J., Wesnousky, S.G., Zhang, P., Slemmons, D.B., 1996: Surface faulting of the 1954 Fairview Peak (Ms7.2) and the Dixie Valley (Ms6.8) earthquakes, Central Nevada. *Bulletin of the Seismological Society of America* 86; 761-787.
- Cole, J.W. and Lewis, K.B., 1981: Evolution of the Taupo-Hikurangi subduction system. *Tectonophysics* 72: 1-21.
- Cooper A.F., and Norris, R.J. 1990. Estimates for the timing of the last coseismic displacement on the Alpine Fault, northern Fiordland, New Zealand. *New Zealand Journal of Geology and Geophysics*, 33 : 303-307.
- Cornell, C.A. 1968: Engineering seismic risk analysis. *Bulletin of the Seismological Society of America* 58: 1583-1606.
- Cousins, W.J., Zhao, J.X, and Perrin, N.D. 1999. A model for the attenuation of peak ground acceleration in New Zealand based on seismograph and accelerograph data, *Bulletin of the New Zealand Society for Earthquake Engineering*. 32: 193-220.
- Crouse, C.B. 1991. Ground-motion attenuation equations for earthquakes on the Cascadia subduction zone, *Earthquake Spectra*, 7 : 201-236.
- Delteil, J.; Collot, J-Y.; Wood, R.; Herzer, R.; Calmant, S.; Christoffel, D.; Coffin, M.; Ferriere, J.; Lamarche, G.; Lebrun, J-F.; Mauffret, A.; Pontoise, B.; Popoff, M.; Ruellan, E.; Sosson, M.; Sutherland, R. 1996: From strike-slip faulting to oblique subduction: a survey of the Alpine Fault-Puysegur Trench transition, New Zealand, results of cruise Geodyn-sud leg 2. *Marine geophysical researches* 18: 383-399.
- DeMets, C., Gordon, R.G., Argus, D.F., and Stein, S. 1994: Current plate motions. *Geophysical Journal International* 101: 425-478.



- Dowrick, D.J., and Rhoades, D.A. 1999: Attenuation of Modified Mercalli intensity for New Zealand earthquakes, *Bulletin of the New Zealand National Society for Earthquake Engineering* 21: 55-89.
- Ellsworth, W. Matthews, M.V., Nadeau, R.M., Nishenko, S.P., Reasenber, P.A., and Simpson, R.W. 1999: A physically-based earthquake recurrence model for estimation of long-term earthquake probabilities (Extended Abstract). *Workshop on Earthquake Recurrence: State of the Art and Directions for the Future*. Instituto Nazionale de Geofisica, Rome, Italy. 22-25 February 1999.
- Fellows, D.L. 1996. *Preliminary paleoseismic assessment of the Wairoa North fault*. ARC Environment Technical Publication No. 75.
- Grapes, R., Little, T., and Downes, G. 1997. The 1855 Wairarapa, New Zealand, Earthquake - Analysis of Historical Data. *Bulletin of the New Zealand National Society for Earthquake Engineering*, 30: 271-368.
- Grapes, R.H., Little, T.A., Browne, Rait, G.J. 1997. *Ngapotiki Thrust, White Rock and Te Kaukau Point, Southeast Wairarapa: Active and inactive structures of the Hikurangi forearc*. Geological Society of New Zealand Annual Conference, November 1997. Field Trip Guide FT2.
- Grapes, R., Little, T., and Downes, G. 1998. Rupturing of the Awaterere Fault during the 1848 October 16 Marlborough earthquake, New Zealand: historical and present day evidence. *New Zealand Journal of Geology and Geophysics* 41:387-399.
- Gutenberg, B. and Richter, C.F. 1944: Frequency of earthquakes in California. *Bulletin of the Seismological Society of America* 34: 185-188.
- Haines, A.J. 1981. A local magnitude scale for New Zealand earthquakes, *Bulletin of the Seismological Society of America*, 71 : 275-294.
- Haines, A.J., Darby, D.J. 1987. *Preliminary dislocation models for the 1931 Napier & 1932 Wairoa earthquakes*. New Zealand Geological Survey report EDS 114.
- Hanks, T.C. and Kanamori, H., 1979: A moment magnitude scale. *Journal of Geophysical Research*, 84: 2348-2350.
- Hanson, S.L., Thenhaus, P.C., Chapman-Wilbert, M. and Perkins, D.M., 1992: *Analyst's manual for USGS seismic hazard programs adapted to the Macintosh computer system*. U.S. Geological Survey Open File Report 92-529.
- Heron, D., Van Dissen, R.H., and Sawa, M. 1998. Late Quaternary movement on the Ohariu Fault, Tongue Point to McKays Crossing, North Island, New Zealand. *New Zealand Journal of Geology and Geophysics* 41 : 419-440.
- Hull, A.G., and Dellow, G.D. 1993 *Earthquake hazards in the Taranaki region*. GNS client report 1993/03.
- Hyndman, R.D., Yamano, M., and Oleskevich, D.A. 1997. The seismogenic zone of subduction thrust faults. *The Island Arc* 6, 244-260.



- Idriss I. M. 1991. *Selection of earthquake ground motions at rock sites*, Report prepared for the Structures Division, Building and Fire Research Laboratory, National Institute of Standards and Technology, Department of Civil Engineering, University of California, Davis.
- Katayama, T. 1982. An engineering prediction model of acceleration response spectra and its application to seismic hazard mapping. *Earthquake Engineering and Structural Dynamics*, 10: 149-163.
- Kelsey, H.M., Hull, A.G., Cashman, S.M., Berryman, K.R., Cashman, P.H. Trexler, J.H., Begg, J.G. 1998. Paleoseismicity of an active reverse fault in a forearc setting : The Poukawa fault zone, Hikurangi forearc, New Zealand. *The Geological Society of America Bulletin* 110 : 1123-1148.
- Lecointre, J.A. Neal, V.E., Pamer, A.S. 1998. Quaternary lahar stratigraphy of the Western Ruapehu ring plain, *New Zealand Journal of Geology & Geophysics* 41 : 221-245.
- Little, T.A., Grapes, R. 1998. Late Quaternary strike-slip on the eastern part of the Awatere fault, South Island, New Zealand. *The Geological Society of America Bulletin* 110 : 127-148.
- Matuschka, T., Berryman, K.R., O'Leary, A.J., McVerry, G.H., Mulholland, W.M. and Skinner, R.I. 1985: New Zealand seismic hazard analysis, *Bulletin of the New Zealand National Society for Earthquake Engineering*, 18 : 313-322.
- Mazengarb, C., Cousins, J., Dellow, G., Townsend, T. 1997. *Earthquake and related hazards in the Gisborne District*. Institute of Geological and Nuclear Sciences Client Report 1997/44692D.13.
- McGinty, P. 1999: Preparation of the New Zealand Seismicity Catalogue for a probabilistic seismic hazard analysis of New Zealand. *Abstracts. New Zealand Geophysical Society and Meteorological Society of New Zealand Joint conference*, Victoria University of Wellington 1-3 September 1999.
- McVerry, G.H., Zhao, J.X., Abrahamson, N.A., Somerville, P.G. 2000. Crustal and subduction zones attenuation relations for New Zealand earthquakes. *Paper No. 1834, Proceedings of the 12th World Conference of Earthquake Engineering 2000*. Auckland, New Zealand.
- Melhuish, A., Sutherland, R., Davey, F.J., Lamarche, G., 1999. Crustal structure and neotectonics of the Puysegur oblique subduction zone, New Zealand. *Tectonophysics* 313: 335-362.
- Mooney, H.M. 1970. Upper mantle inhomogeneity beneath New Zealand: seismic evidence, *Journal of Geophysical Research*, 75 : 285-309.
- Mulholland, W.M. 1982. *Estimation of design earthquake motions for New Zealand*. Research Report 82-9. Department of Civil Engineering, University of Canterbury.
- National Earthquake Hazard Reduction Program (NEHRP) 1994. *1994 Recommended Provisions for Seismic Regulations of New Buildings: Part 1, Provisions*, issued by Federal Emergency Management Agency, FEMA 222A, 290 pp.



- New Zealand Geomechanics Society 1998. *Guidelines for the field descriptions of soils and rocks in engineering use.*
- Nicol, A and Van Dissen, R.J. 1997. *Late Miocene to recent fault and fold deformation east of Martinborough, Wairarapa.* Geological Society of New Zealand annual conference, November 1997. Field Trip Guide FT3.
- Peek, R. 1980. *Estimation of seismic risk for New Zealand. A seismicity model and preliminary design spectra.* Research report 80-21, Department of Civil Engineering, University of Canterbury.
- Peek, R., Berrill, J.B. and Davis, R.O. 1980. A seismicity model for New Zealand. *Bulletin of the New Zealand National Society for Earthquake Engineering*, 13: 355-364.
- Pettinga, J.R., Chamberlain, C.G., Yetton, M.D., Van Dissen, R.J., and Downes, G., 1998. *Earthquake Hazard and Risk Assessment Study (Stage 1 – Part A); Earthquake Source Identification and Characterisation.* Canterbury Regional Council Publication U98/10.
- Reasenbergs, P. 1985. Second-order moment of central California seismicity, 1969-1982. *Journal of Geophysical Research* 90: 5479-5496.
- Reiter, L. 1991. *Earthquake hazard analysis. Issues & insights.* Columbia University Press. 253pp.
- Reyners, M. 1983: Lateral segmentation of the subducted plate at the Hikurangi margin, New Zealand: seismological evidence. *Tectonophysics* 96: 203-223.
- Reyners, M. 1998: Plate coupling and the hazard of large subduction thrust earthquakes at the Hikurangi subduction zone, New Zealand. *New Zealand Journal of Geology and Geophysics* 41: 343-354.
- Reyners, M. 1999: Quantifying the hazard of large subduction thrust earthquakes in Hawkes Bay. Abstracts. *New Zealand Geophysical Society and Meteorological Society of New Zealand Joint Conference*, Victoria University of Wellington 1-3 September 1999.
- Reyners, M., Robinson, R., & McGinty, P. 1997. Plate coupling in the northern South Island and southernmost North Island, New Zealand, as illuminated by earthquake focal mechanisms. *Journal of Geophysical Research* 102 : 15197-15210.
- Rhoades, D.A. 1996. Estimation of the Gutenberg-Richter relation allowing for individual earthquake magnitude uncertainties. *Tectonophysics*, 258 : 71-83.
- Sadigh, K., Chang, C.-Y., Egan, J.A., Makidisi, F. and Youngs, R.R. (1997). Attenuation relationships for shallow crustal earthquakes based on Californian strong motion data, *Seismological Research Letters*, 68 : 180-189.
- Schermer, E., Van Dissen, R.J., Berryman, K.R., 1999. *In search of the source of the 1934 Pahiatua earthquake.* Final report on EQC Research project 97/320.71 pp.
- Smith, W.D. and Berryman, K.R. 1983. Revised estimates of earthquake hazard in New Zealand. *Bulletin of the New Zealand National Society for Earthquake Engineering*. 16 : 259-276.



- Smith, W.D. and Berryman, K.R. 1986: Earthquake hazard in New Zealand: inferences from seismology and geology. *Bulletin of the Royal Society of New Zealand* 24: 223-243.
- Somerville, P.G., Sato, T., Ishii, T. 1999: Characterising subduction earthquake slip models for the prediction of strong ground motion. *EOS Transactions, American Geophysical Union 1998 Fall Meeting* 79(46), F658.
- Standards New Zealand, 1992. *Code for Practice for General Structural Design and Design Loadings for Buildings. Volume 1: Code of practice. NZS 4203:1992.*
- Stirling, M.W., Wesnousky, S.G. and Shimazaki, K. 1996. Fault trace complexity, cumulative slip, and the shape of the magnitude-frequency distribution for strike-slip faults: a global survey. *Geophysical Journal International* 124: 833-868.
- Stirling, M.W., Wesnousky, S.G. and Berryman, K.R., 1998. Probabilistic seismic hazard analysis of New Zealand. *New Zealand Journal of Geology and Geophysics* 41: 355-375.
- Stirling, M.W., Yetton, M., Pettinga, Y., Berryman, K.R., Downes, G. 1999. *Probabilistic seismic hazard assessment and earthquake scenarios for the Canterbury region, and historic earthquakes in Christchurch. Stage 1 (Part B) of Canterbury Regional Council's earthquake hazard and risk assessment study.* Institute of Geological and Nuclear Sciences Client Report 1999/53.
- Sutherland, R.; Norris, R. J. 1995: Late Quaternary displacement rate, paleoseismicity and geomorphic evolution of the Alpine Fault: Evidence from near Hokuri Creek, south Westland, New Zealand. *New Zealand journal of Geology and geophysics* 38: 419-430.
- Sutherland, R. 1999. Cenozoic bending of New Zealand basement terranes and Alpine Fault displacement: a brief review. *New Zealand Journal of Geology and Geophysics* 42 : 295-301.
- Turnbull, I.M., Uruski, C.I. and others, 1993. *Cretaceous and Cenozoic sedimentary basins of western Southland, South Island, New Zealand.* Institute of Geological and Nuclear Sciences, Ltd. Monograph 1 (New Zealand Geological Survey basin studies 4), Wellington.
- Turnbull, I.M., Uruski, C.I. 1995. *Geology of the Monowai-Waitutu area, scale 1:50,000.* Institute of Geological and Nuclear Sciences geological map 19, Lower Hutt, New Zealand.
- Van Dissen, R.J., Begg, J. Palmer, A., Nicol, A., Darby, D., and Reyners, M. 1998. Newly discovered active faults in the Wellington region. *New Zealand National Society for Earthquake Engineering Technical Conference and AGM*, pp. 1-7. Wairakei, Taupo, March 1998.
- Van Dissen, R.J. and Palmer, A.S. 1998. Northern Ohariu fault. A newly discovered active strike-slip fault in Horowhenua, New Zealand. Geological Society of New Zealand Miscellaneous Publication 101A. *Geological Society of New Zealand Annual Conference*, Christchurch 1998, p234.



- Van Dissen, R, and Nicol, A. 1998 . Paleoseismicity of the middle Clarence Valley section of the Clarence fault, Marlborough, New Zealand. *Programme & abstracts, Geological Society of New Zealand & New Zealand Geophysical Society Joint Annual Conference. Geological Society of New Zealand miscellaneous publication 101B : 233.*
- Van Dissen, R.J., Lindqvist, J.K. and Turnbull, I.M. 1993. *Earthquake hazards in the Southland region.* Institute of Geological and Nuclear Sciences Client Report 1993/66.
- Villamor, P. and Berryman, K. (in review). A Late Quaternary extension rate in the Taupo Volcanic Zone, New Zealand, derived from fault slip data, to be submitted to *New Zealand Journal of Geology and Geophysics.*
- Villamor, P., Van Dissen, R.J., and Downes, G. 1998. *Moawhango dam stability analysis Task 2 Seismic source characterisation.* GNS Client report 43812B.11.
- Weichert, D.H. 1980 : Estimation of the earthquake recurrence parameters for unequal observation periods for different magnitudes. *Bulletin of the Seismological Society of America.* 70: 1337-1346.
- Wells, D.L., and K.J. Coppersmith 1994. New empirical relationships among magnitude, rupture length, rupture width, rupture area, and surface displacement. *Bulletin of the Seismological Society of America* 84: 974-1002.
- Wesnousky, S.G. 1986. Earthquakes, Quaternary faults and seismic hazard in California. *Journal of Geophysical Research* 91: 12587-12631.
- Wood, R.A., Herzer, R., Sutherland, R., Melhuish, A. 2000. Cretaceous-Tertiary tectonic history of the Fiordland margin, New Zealand. *New Zealand Journal of Geology and Geophysics*, in press.
- Woodward Clyde and Institute of Geological and Nuclear Sciences 1999 : *Waitaki River Power Stations. Seismic Loads Assessment.* Draft Client report for Electricity Corporation of New Zealand.
- Yetton, M.D., Wells, A., and Traylen, N.J. 1998. *The probability and consequences of the next Alpine Fault earthquake.* EQC Research Report 95/193.
- Youngs, R.R., Chiou, S.-J., Silva, W.J., and Humphrey, J.R. 1997. Strong ground motion attenuation relationships for subduction zone earthquakes, *Seismological Research Letters*, 68 : 58-73.
- Zhao, J.X., Dowrick, D.J., and McVerry, G.H. 1997. Attenuation of peak ground accelerations in New Zealand earthquakes. *Bulletin of the New Zealand National Society for Earthquake Engineering.* 30 : 133-158.

FIGURES

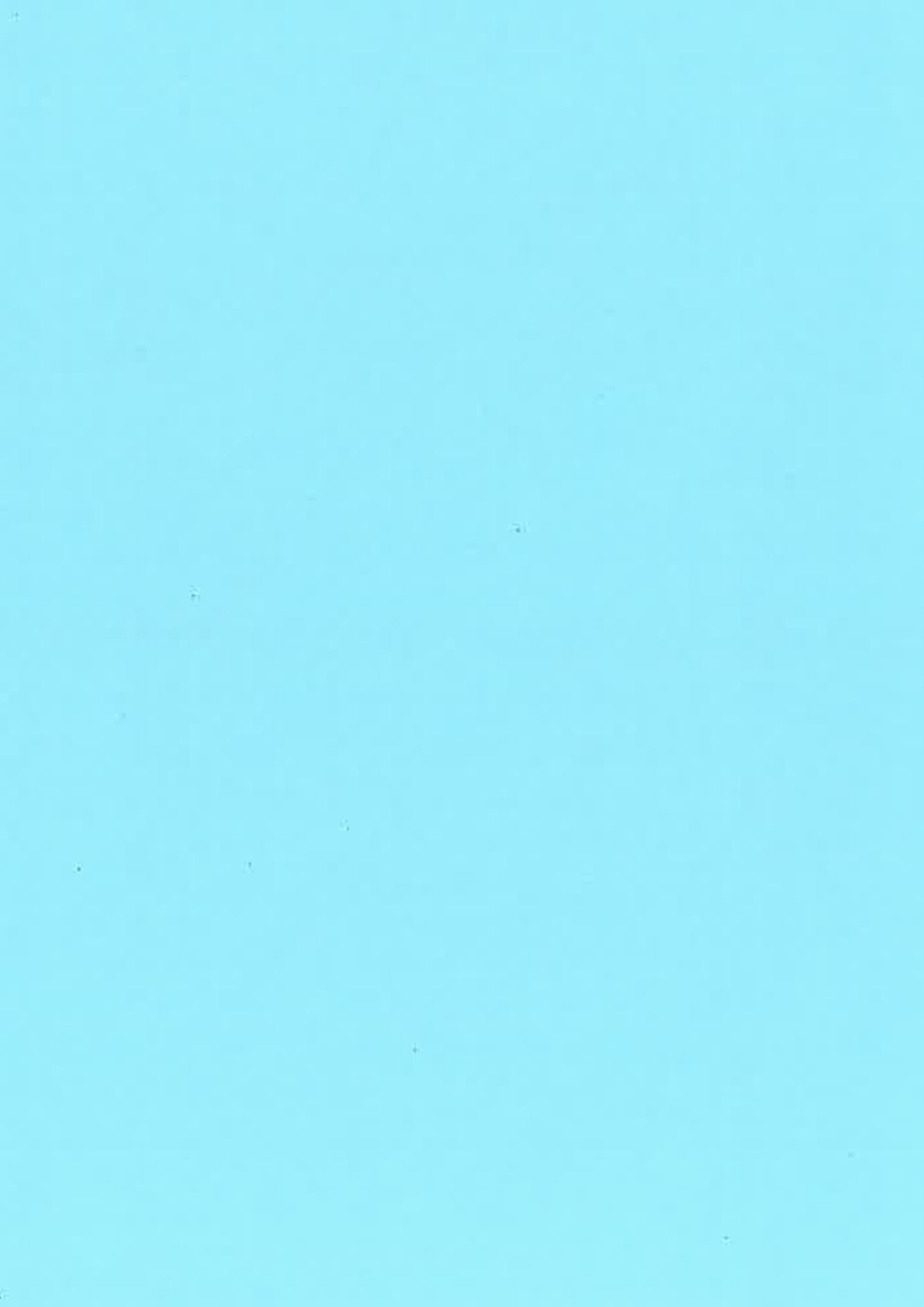


FIGURE CAPTIONS

- Figure 1:** The plate tectonic setting of New Zealand. The country is divided into the neotectonic provinces identified by Berryman and Beanland (1988).
- Figure 2:** The 305 active fault sources used as input for the PSHA. The numbers beside each fault correspond to the index numbers given in the fault table (Appendix 1).
- Figure 3:** The distribution of shallow crustal seismicity in New Zealand (a), and the deeper seismicity of the Fiordland and Hikurangi subduction zones (b). The seismotectonic zones we have defined to sort the catalogue, assign initial regional maximum cutoff magnitudes (M_{cutoff}), and calculate parameter b of the Gutenberg-Richter relationship for seismicity are shown in (a). In the case of (b), many of the deep zones overlap in plan view, so we show the seismicity of each zone as a particular colour, rather than trying to colour-code the actual zones. The vertical extents of the seismotectonic zones have been defined from the spatial and depth distribution of seismicity, and are shown on each plot as a depth range beside the zone number (e.g. "z20 10-45 km" indicates that zone 20 has a depth range of 10 to 45 km). Since the crustal and deep sources have been defined at different scales, the lower-depth-limit of a crustal zone sometimes overlaps with the upper-depth-limit of a deep zone. In these cases the seismicity parameters calculated for the crustal zones are assumed to represent the seismicity of the overlapping areas. In (c) we show the seismicity for the three different time periods of completeness for events of all depths from 1900 to 1997, and cross sections of seismicity across and beneath the country. See the locations of the cross sections on the "Magnitude 6.5" map. Cross sections are oriented with the northwest end to the left of the page. Maps and cross sections in (c) are taken from McGinty (1999).
- Figure 4:** Contours of (a)-(e) the maximum-likelihood cumulative number of events per year for $M \geq 4$, calculated from three catalogue completeness levels and magnitudes ($M \geq 4$ since 1964, $M \geq 5$ since 1940, and $M \geq 6.5$ since 1840); (f)-(j) parameter b of the Gutenberg-Richter relationship $\text{Log}N = A - bM$, and; (k) the maximum "cutoff" magnitude (M_{cutoff}) assumed for distributed earthquakes, for various depth layers beneath the country. The contours have been made over a gridwork of N , b and M_{cutoff} that have been smoothed with a Gaussian smoothing function, in which the correlation distance (standard deviation) is set to 50 km. Since M_{cutoff} for all of the deep seismotectonic zones is set to 7, we only show a contour plot of M_{cutoff} for the crustal (20 km) depth layer. Note that white areas on the b value plots are where no seismicity exists in the depth range shown.
- Figure 5:** (a)-(f). Probabilistic seismic hazard maps for New Zealand for site class B (intermediate soil). The maps show the levels of p_{ga} and 5% damped response spectral acceleration (0.2 and 1s period) with return periods of 475 years (i.e. 10% probability in 50 years) and 1000 years (10% probability in 105 years).
- Figure 6:** Seismic hazard curves for site class B of the annual rate of exceedance for various levels of p_{ga} (a), and 5% damped response spectral acceleration (1s period; b) at the centres of Auckland, Wellington, Christchurch, Dunedin and Otira. Otira is included in the plots as a useful comparison to the main centres, since it is located in the area of highest hazard in the country (Fig. 5).
- Figure 7:** Response spectra for Auckland, Wellington, Christchurch, Dunedin and Otira, for 475 and 1000 year return periods for site class B.
- Figure 8:** Disaggregation plots for Auckland, Wellington, Christchurch, Dunedin and Otira. The plots show the percentage contribution to the 475 and 1000 year levels of hazard (Fig. 7) of the various magnitudes and source-to-site distances of earthquake sources in the model. The plots are produced for p_{gas} and 1s spectral accelerations for site class B.
- Figure 9:** Comparison of the 475 year return period spectra for the five centres obtained in this study (NHM), and the Matuschka et al. (1985) study, and by using the modified Katayama attenuation model of the 1985 study with our NHM seismicity model.

Figure 1

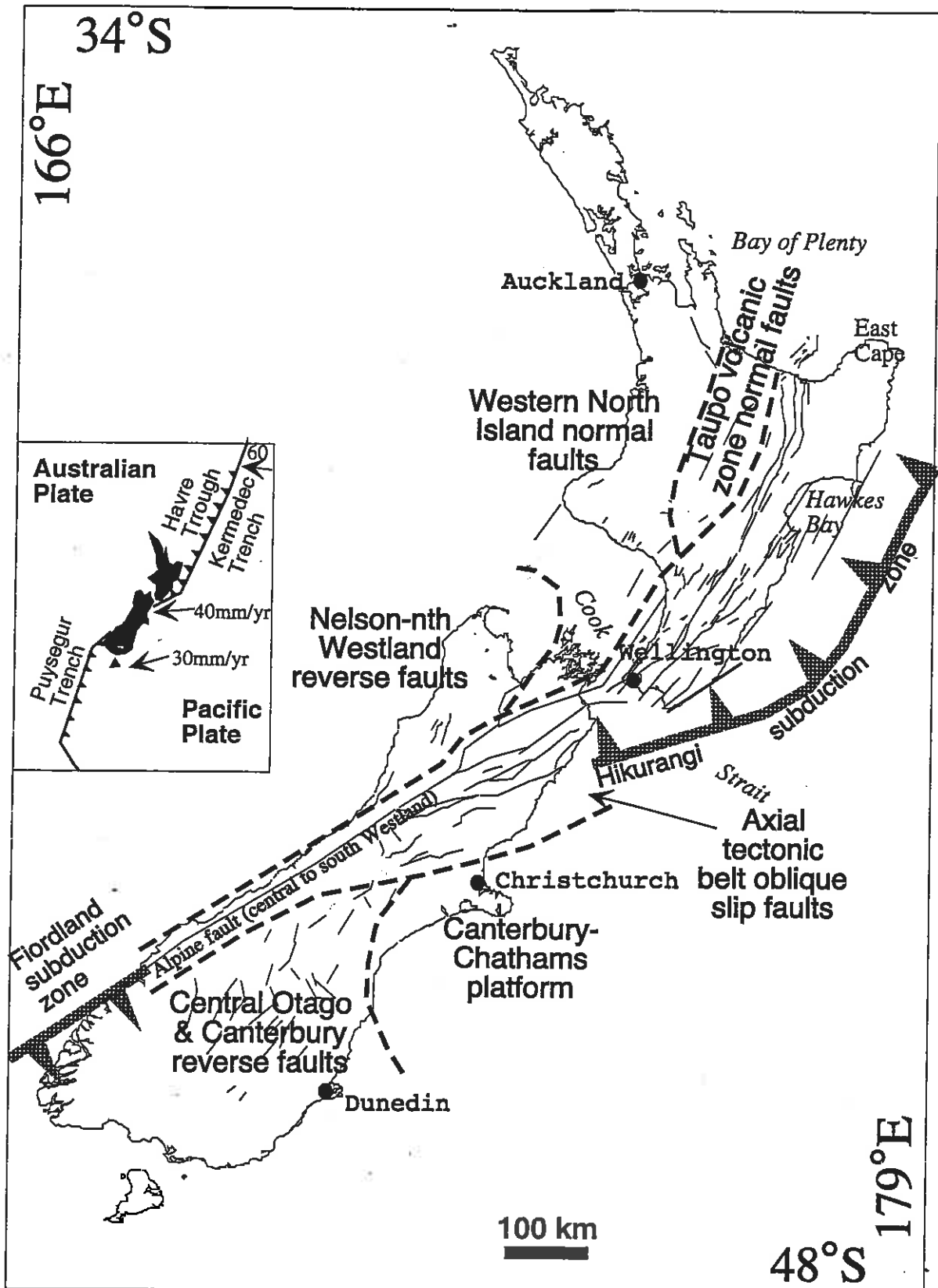


Figure 2a

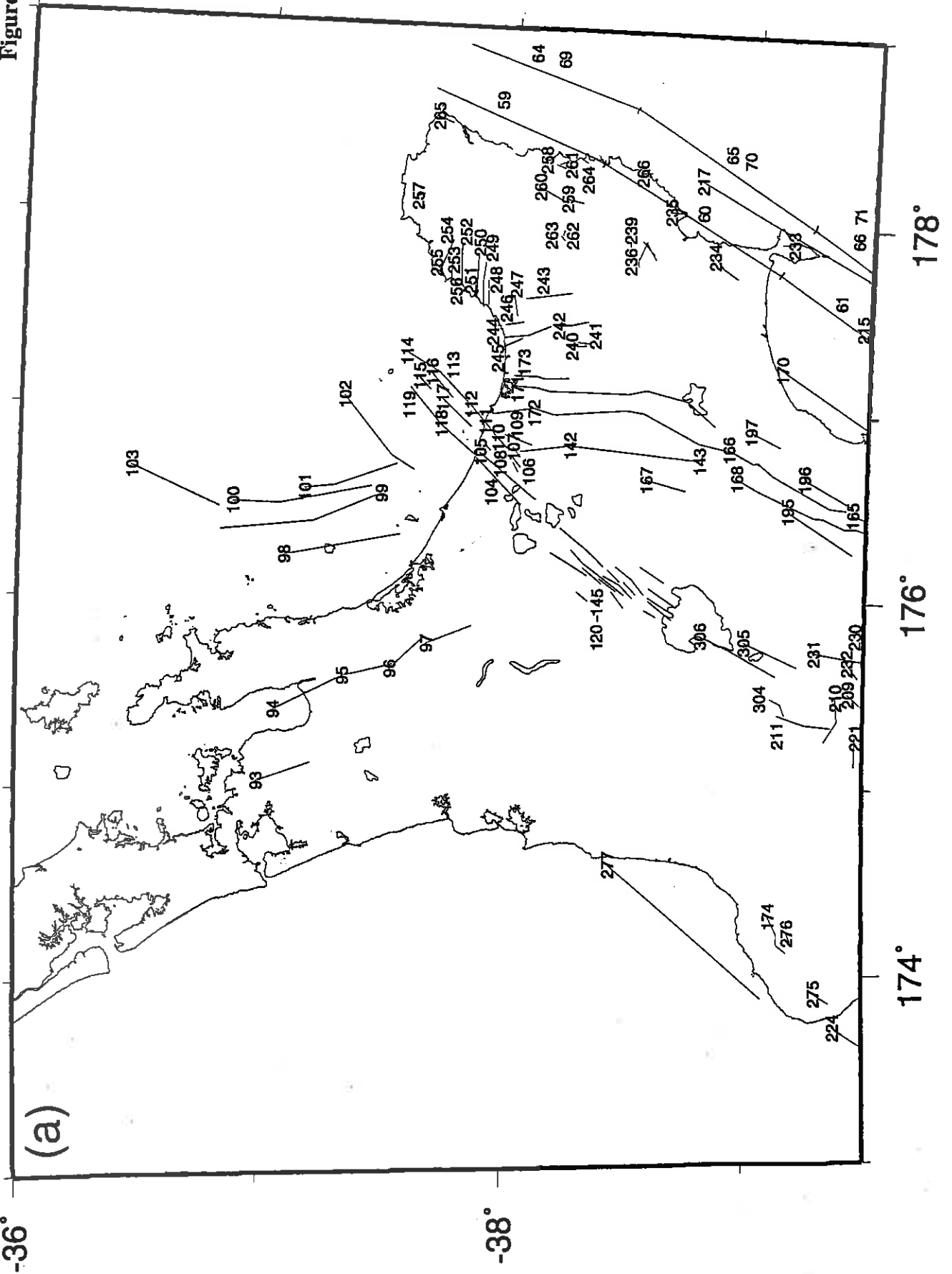


Figure 2c

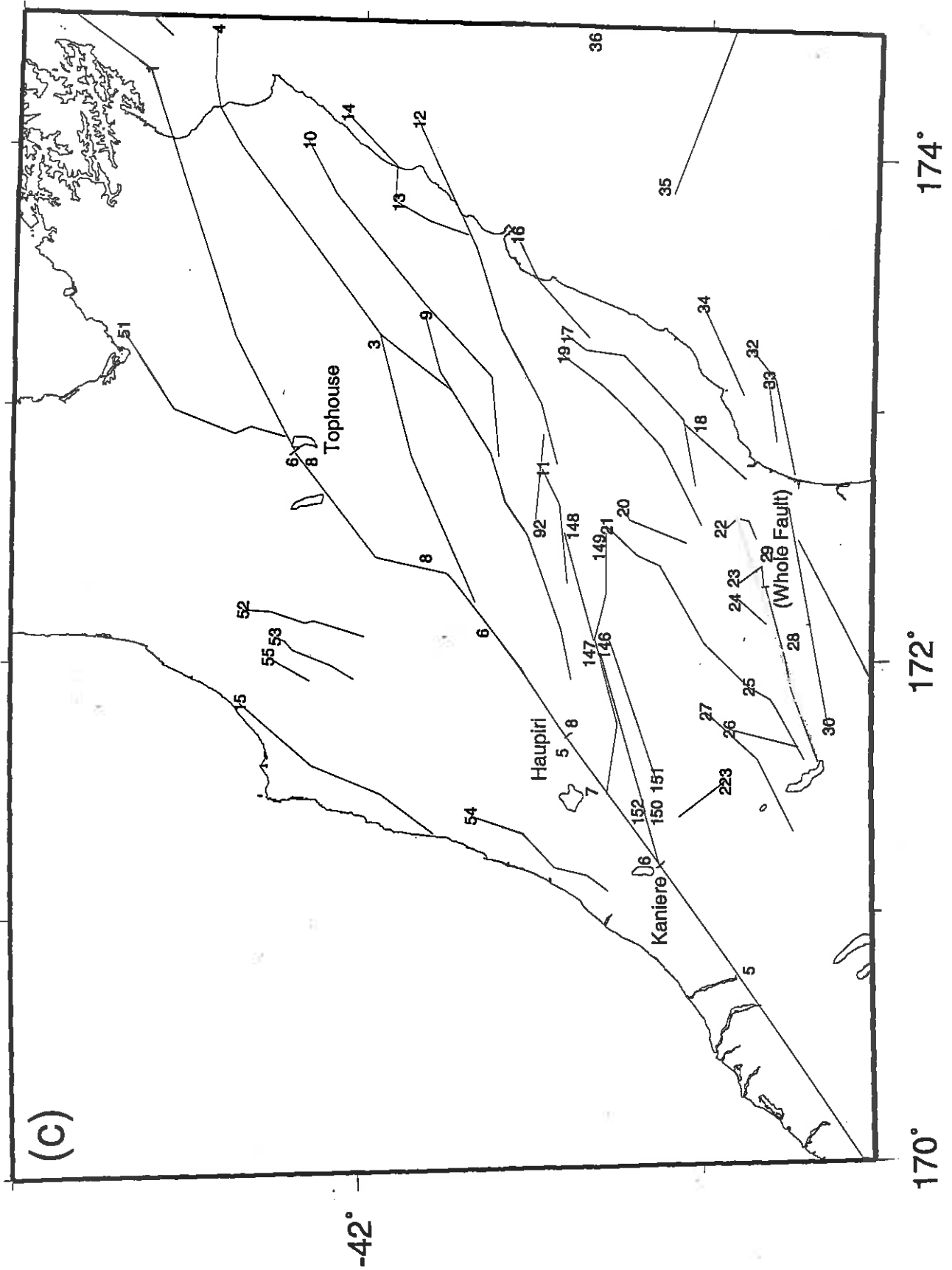


Figure 2d

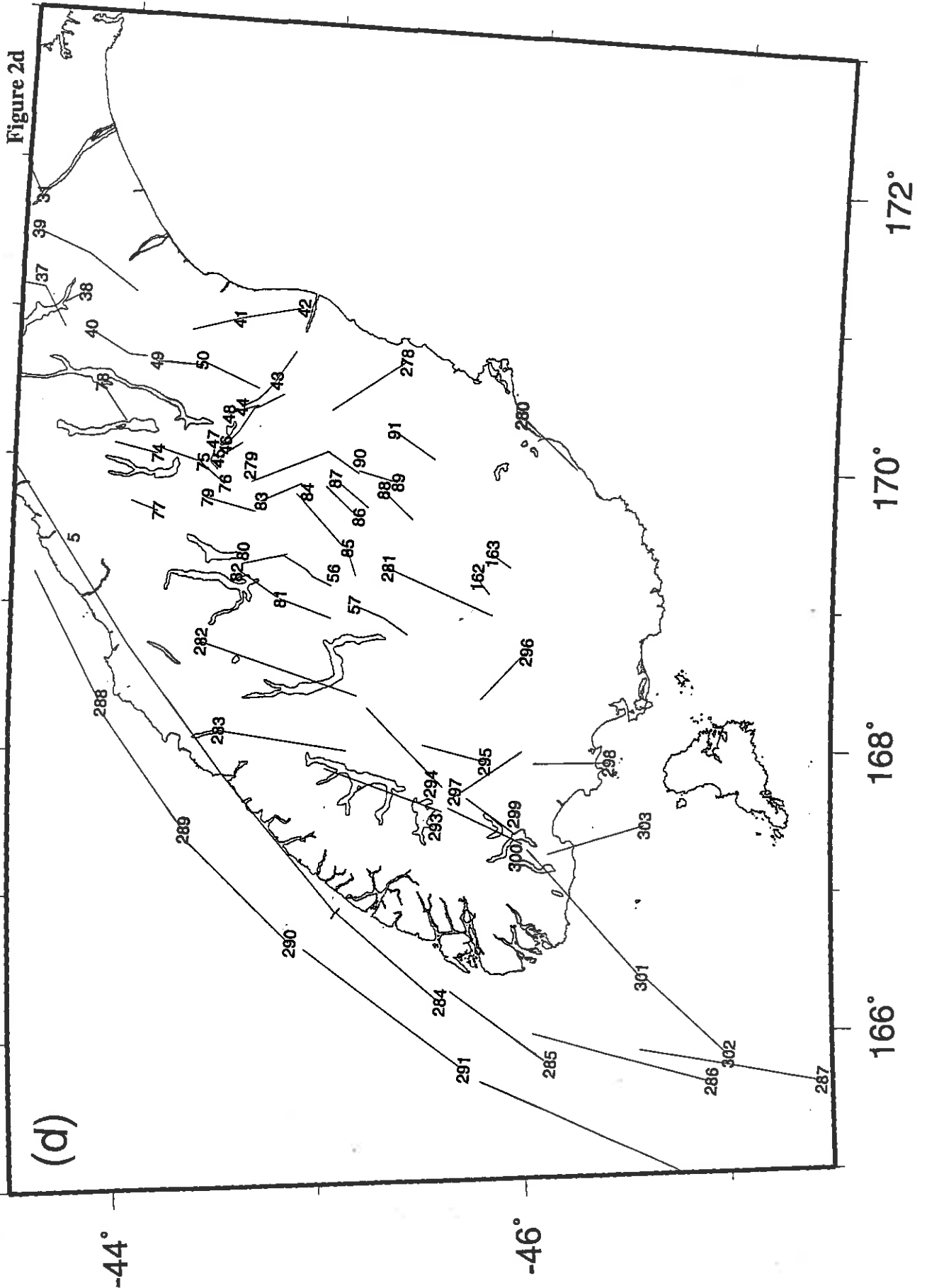


Figure 3a

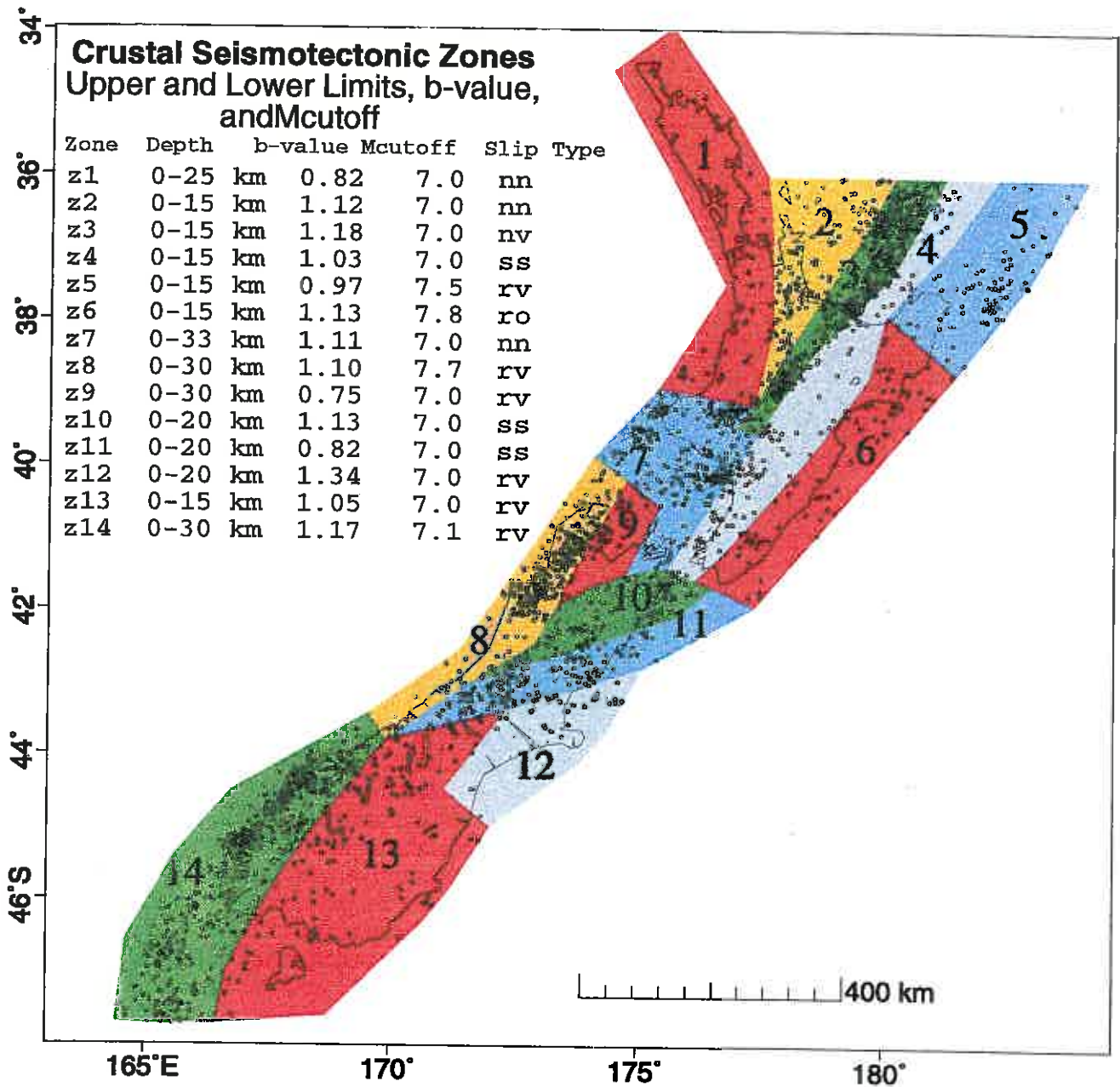


Figure 3b

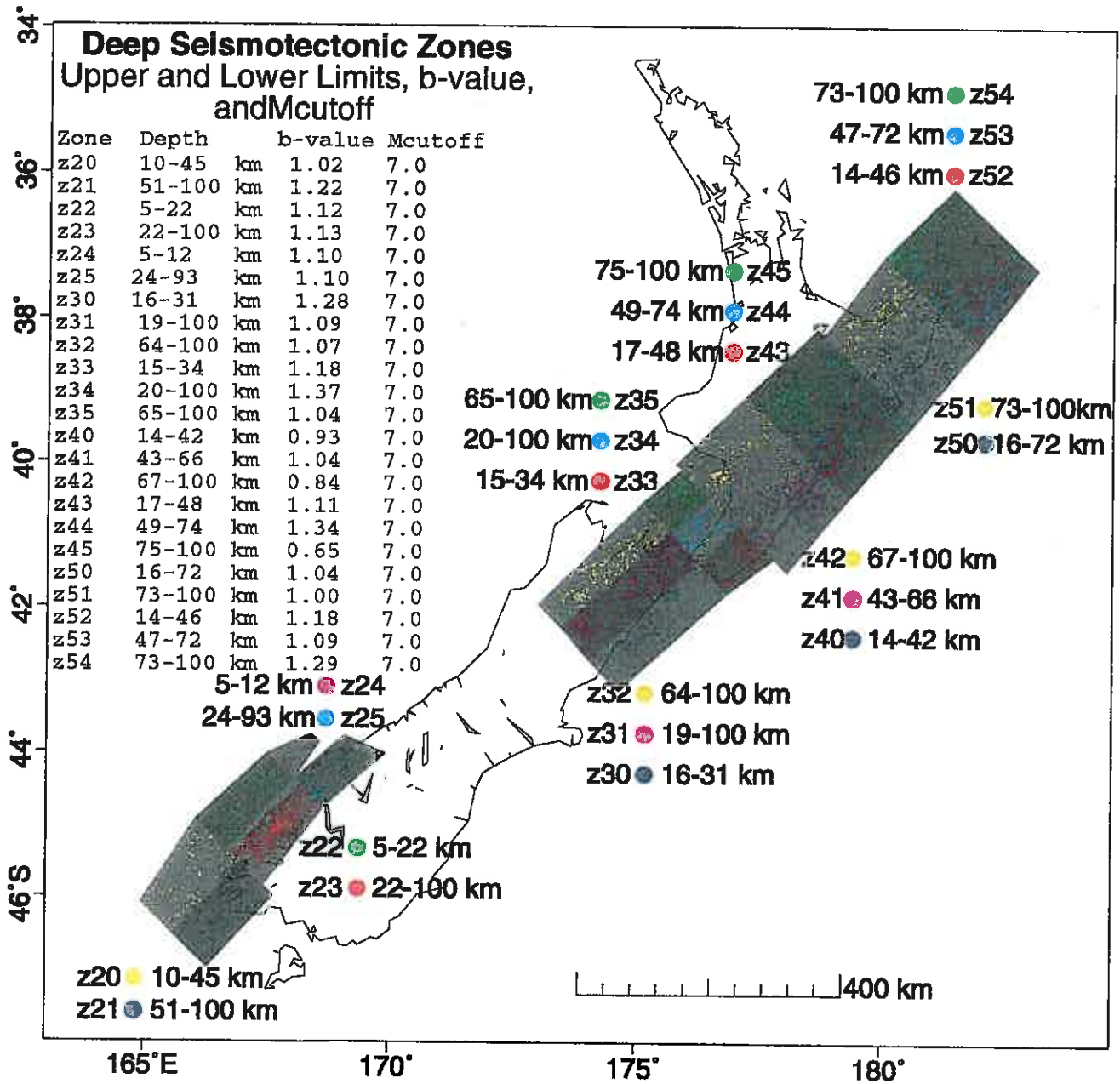


Figure 3c

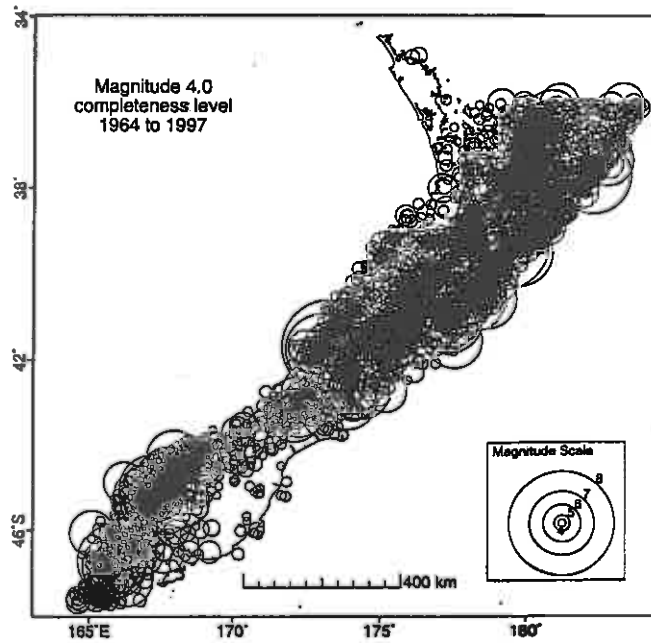
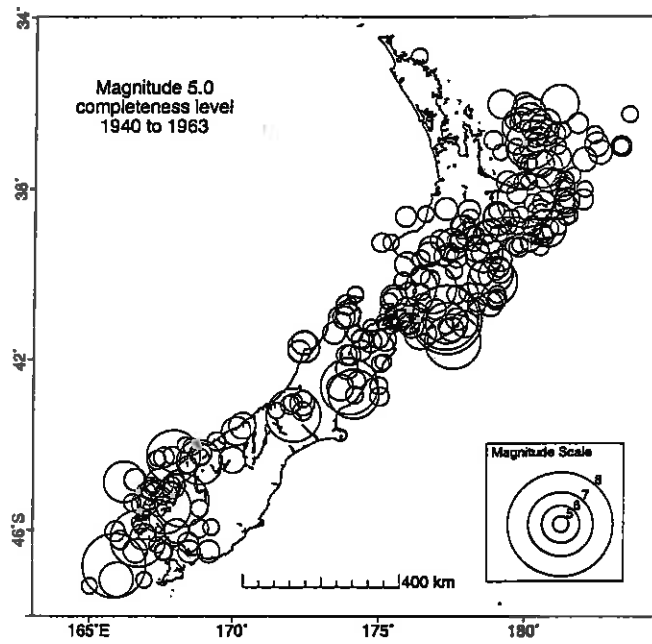
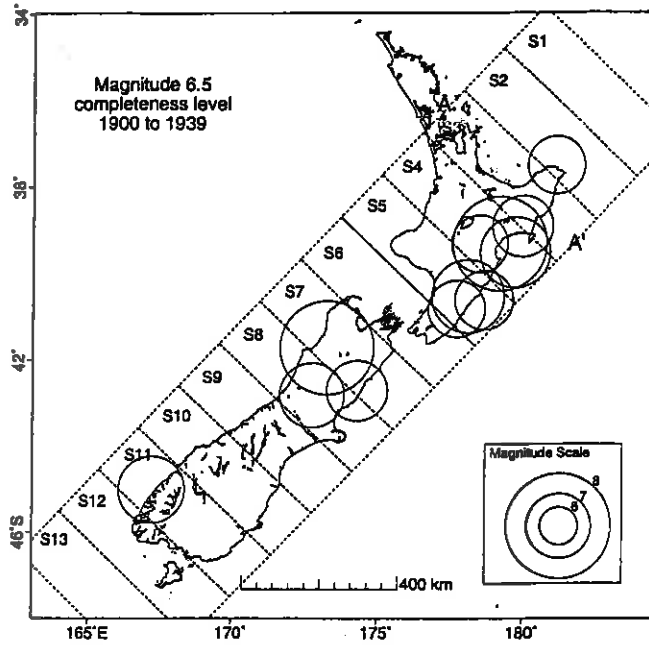
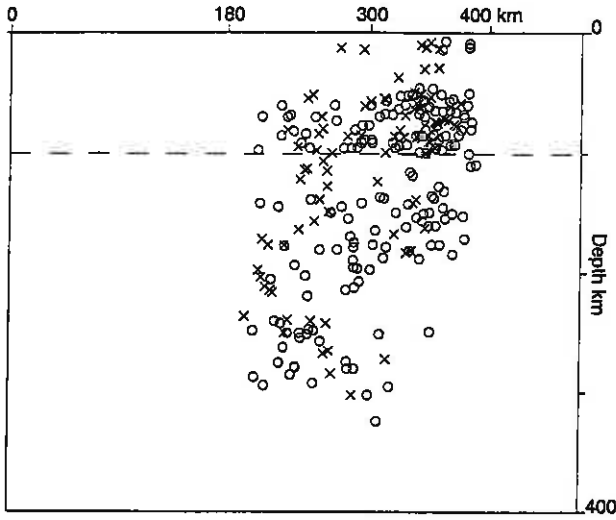
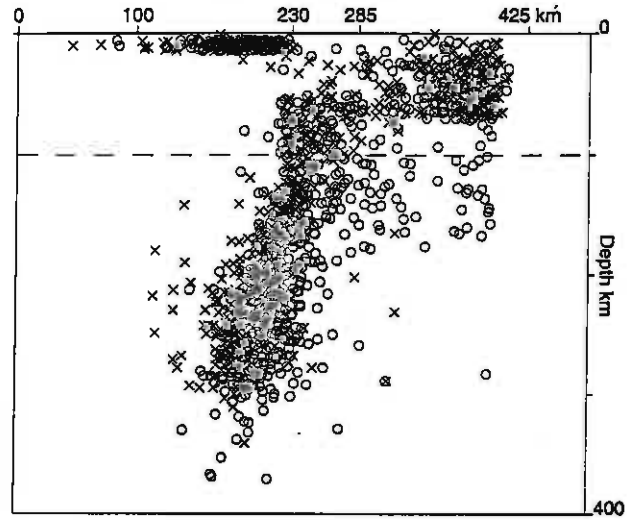


Figure 3c continued

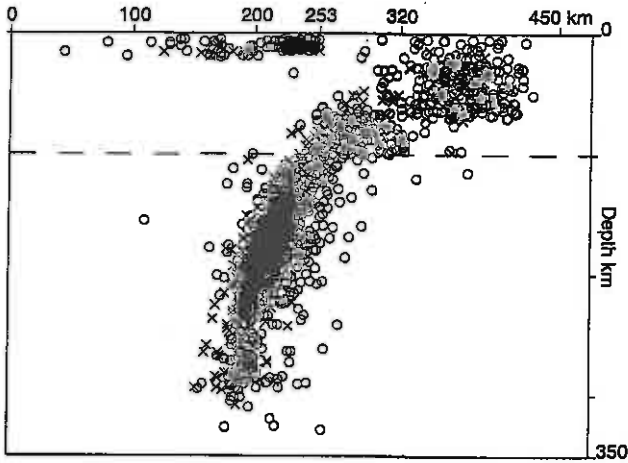
Cross Section 1



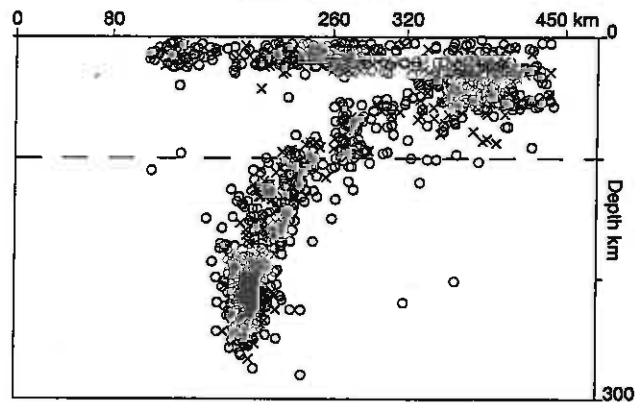
Cross Section 2



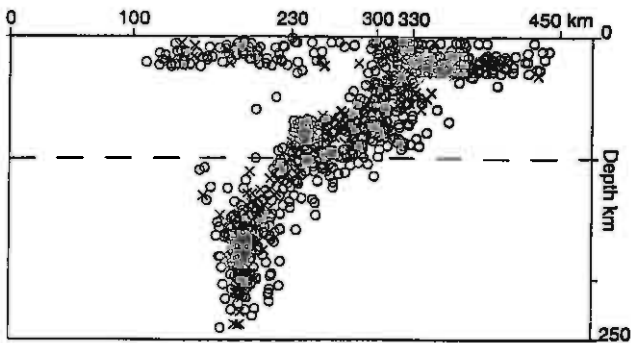
Cross Section 4



Cross Section 5



Cross Section 6



Cross Section 7

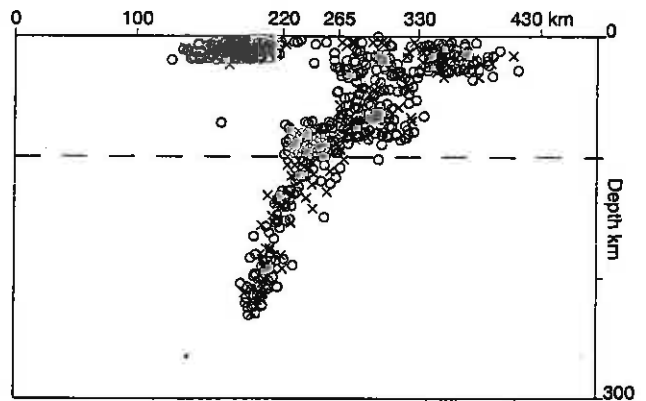


Figure 3c continued

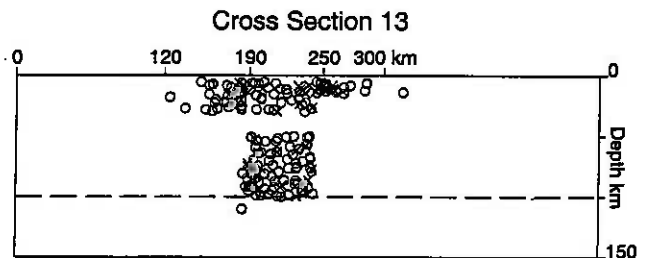
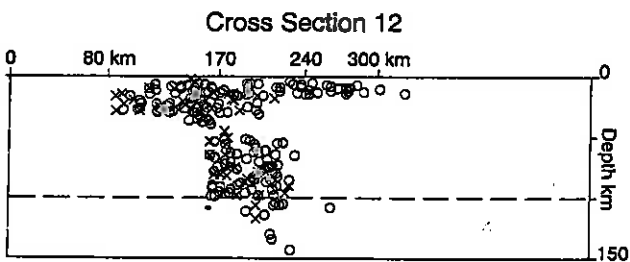
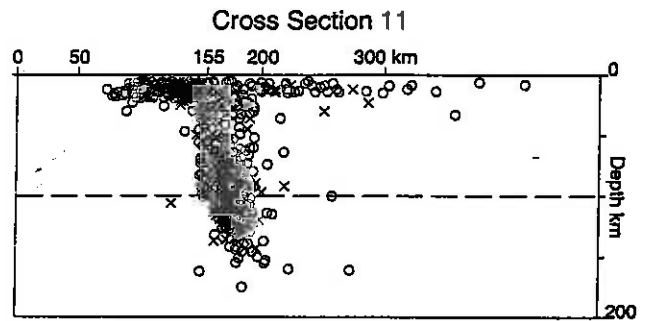
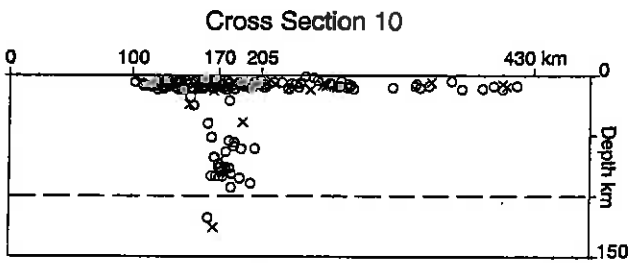
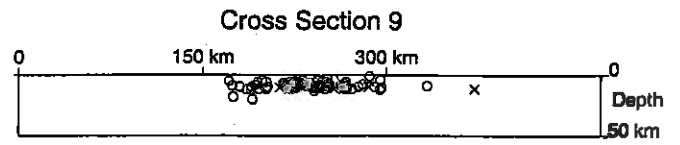
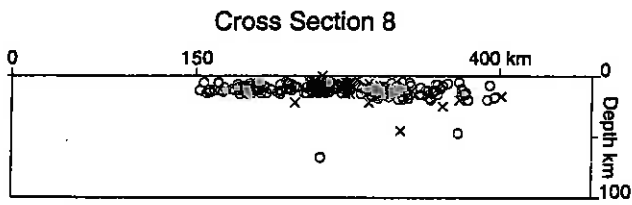


Figure 4a

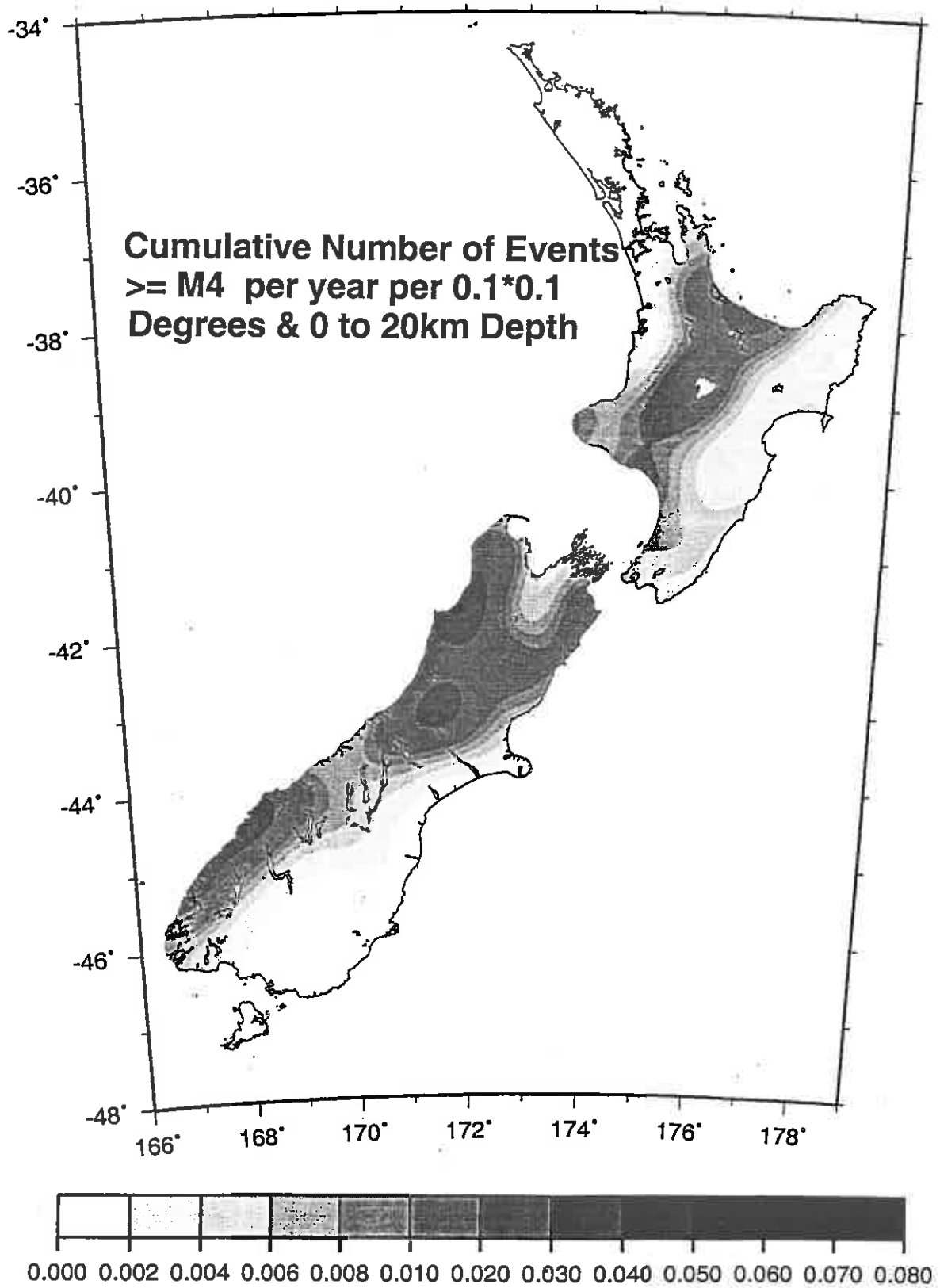


Figure 4b

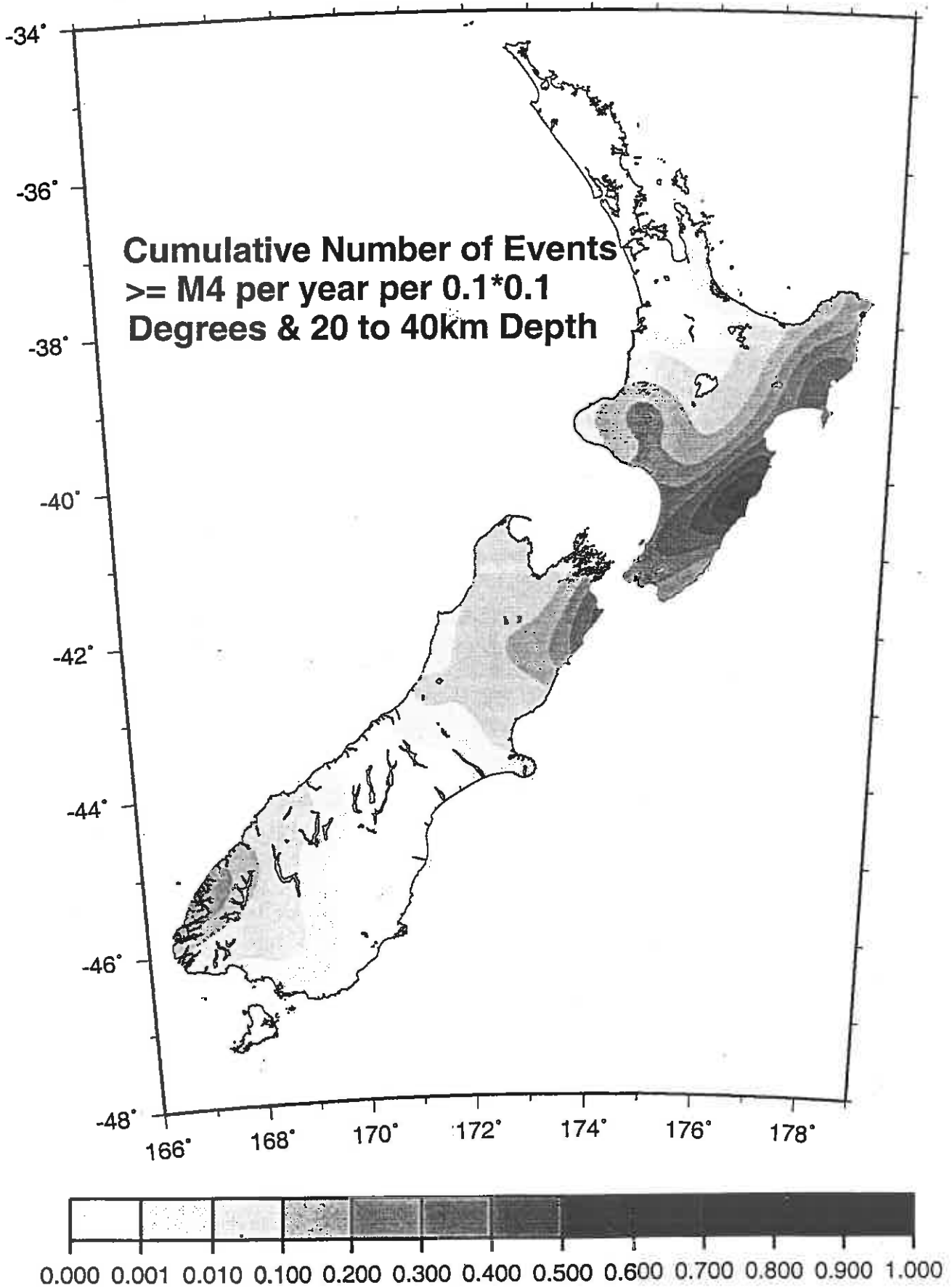


Figure 4c

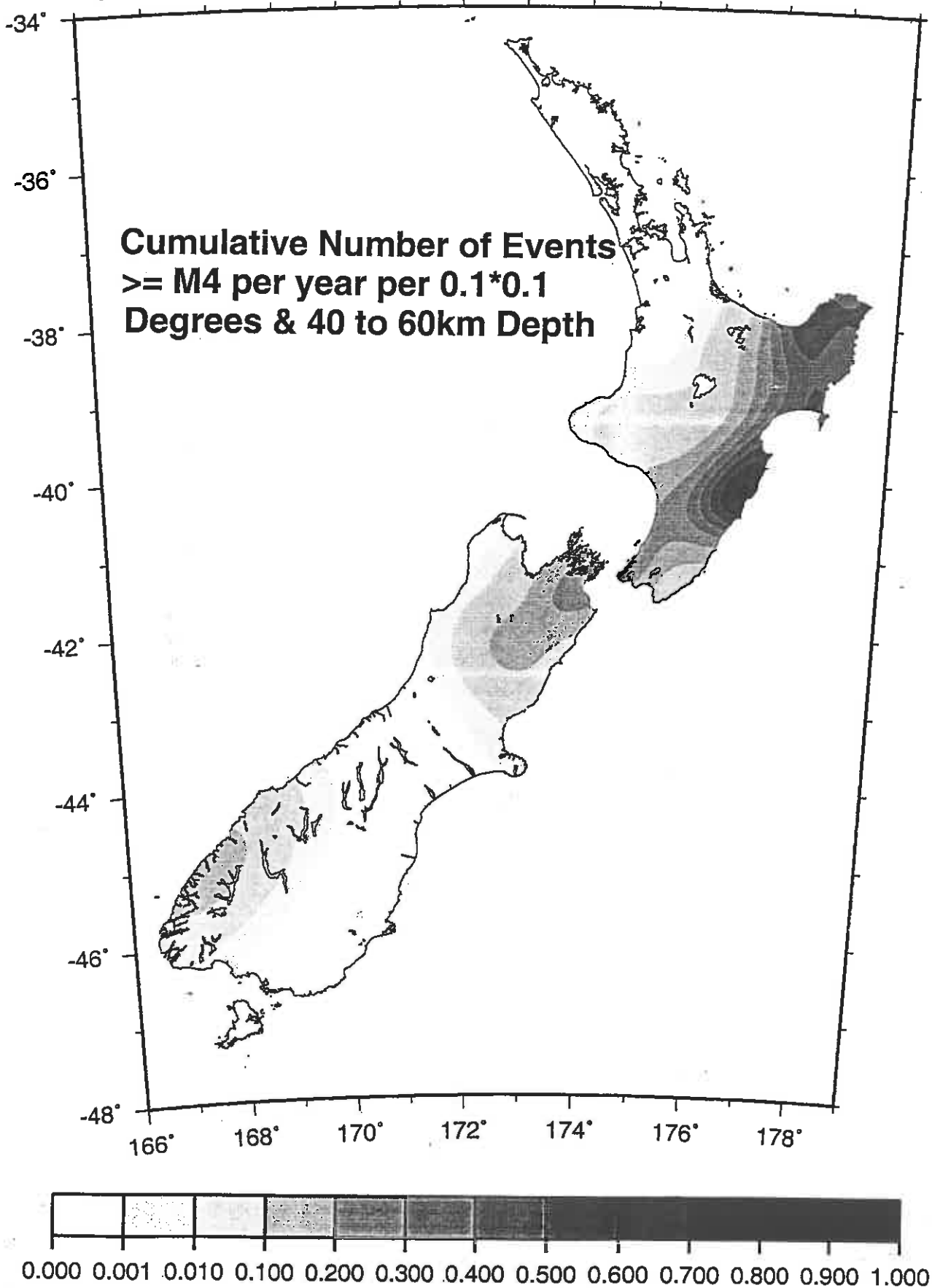


Figure 4d

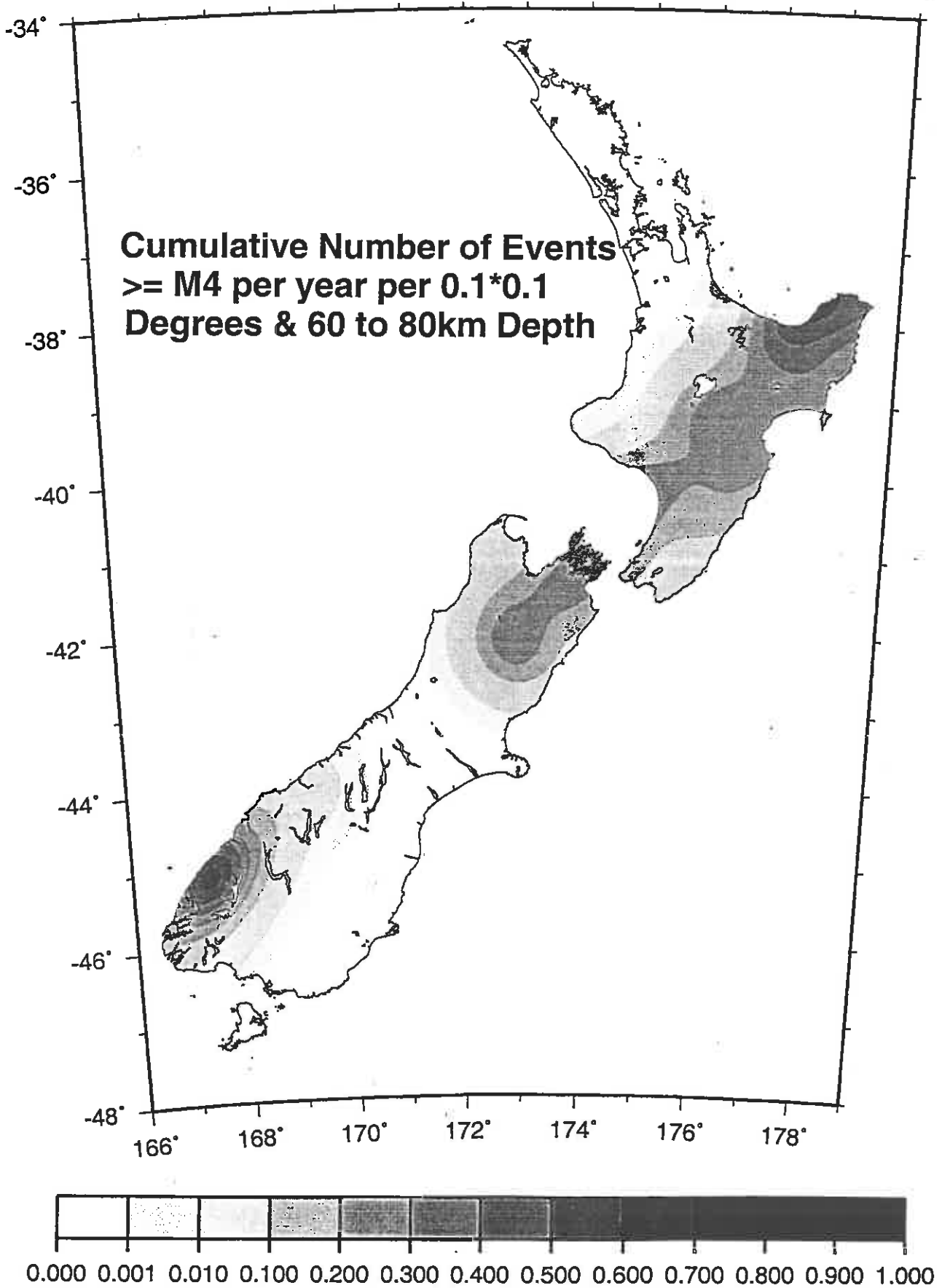


Figure 4e

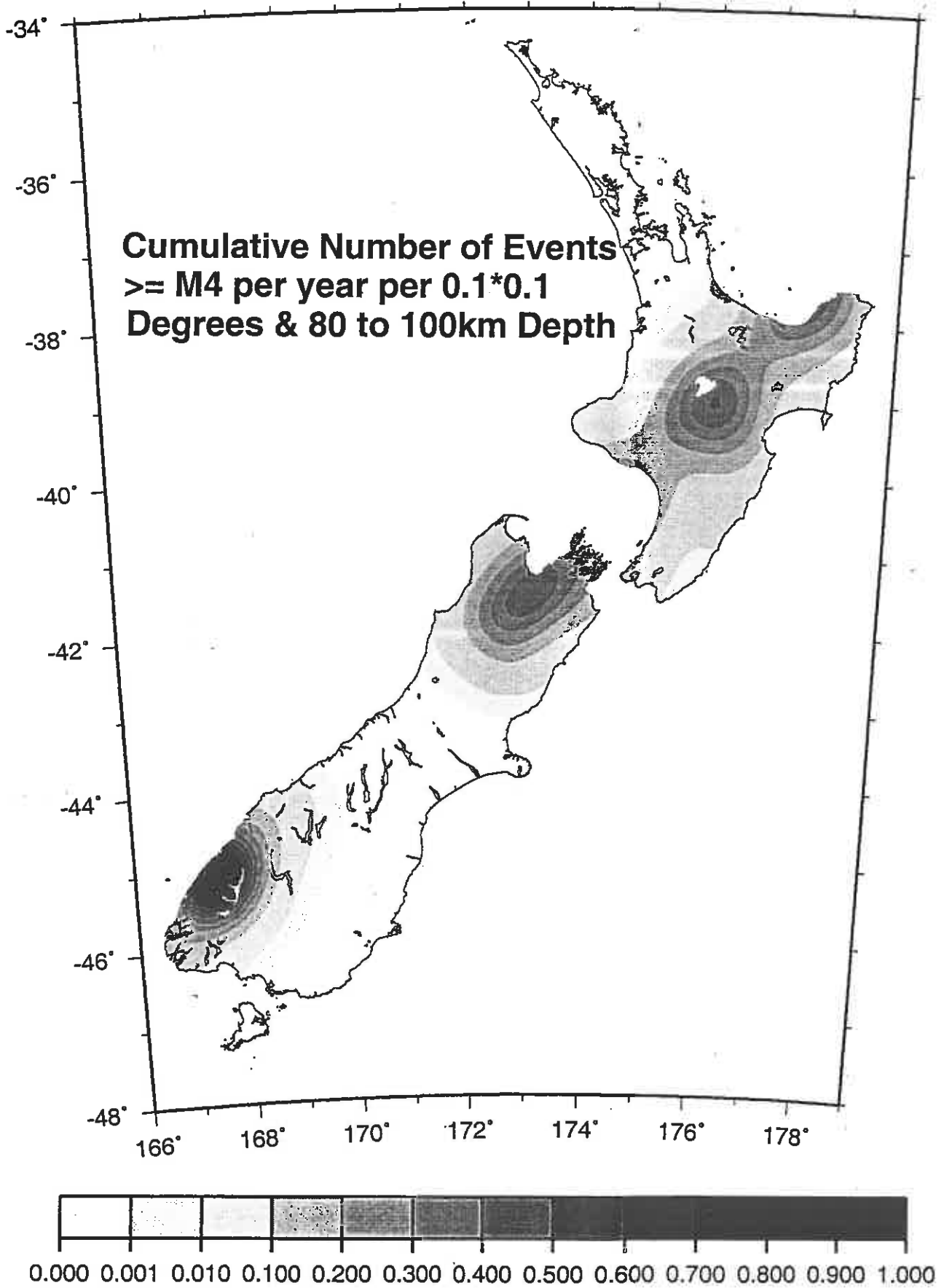


Figure 4f

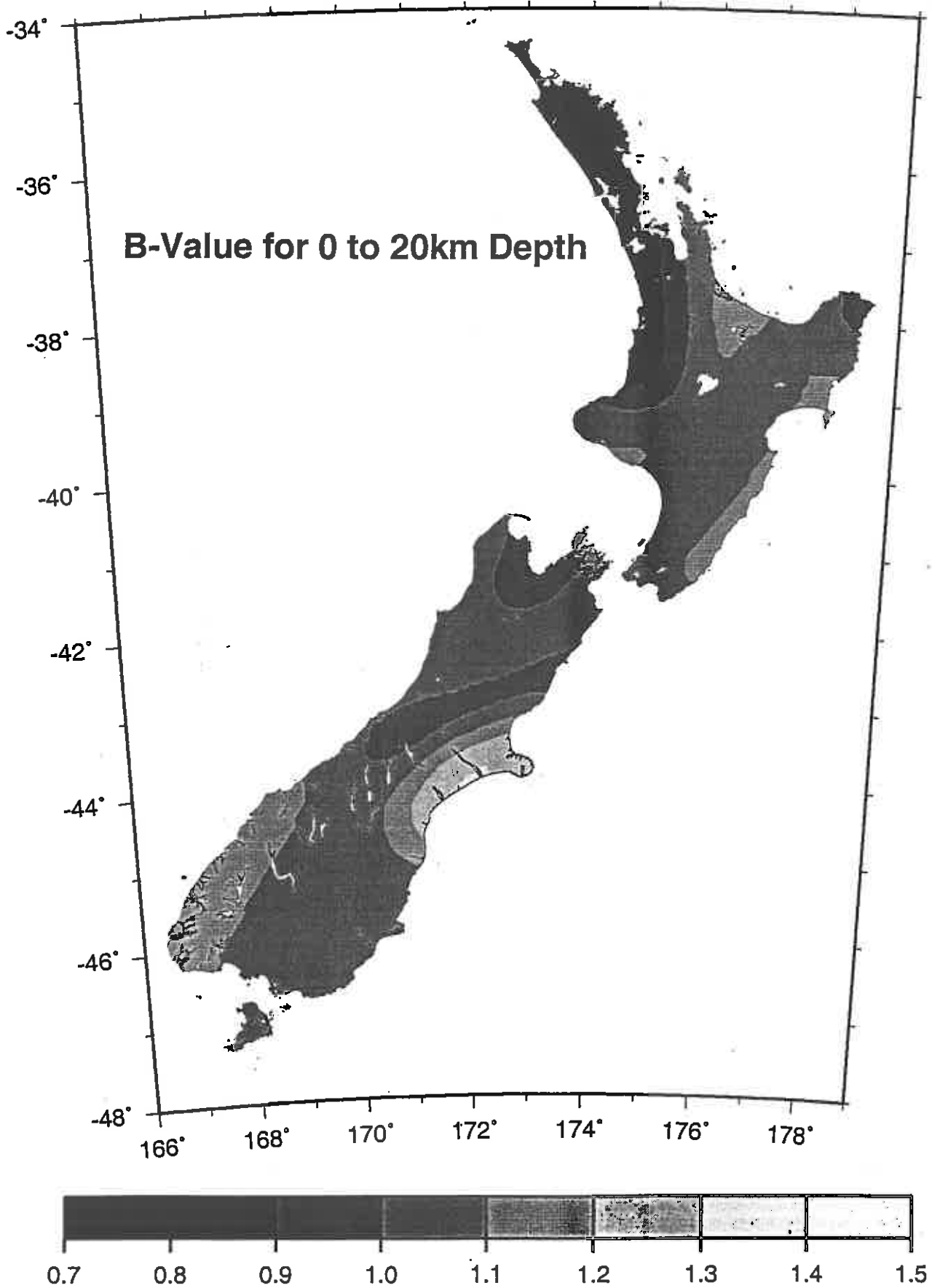


Figure 4g

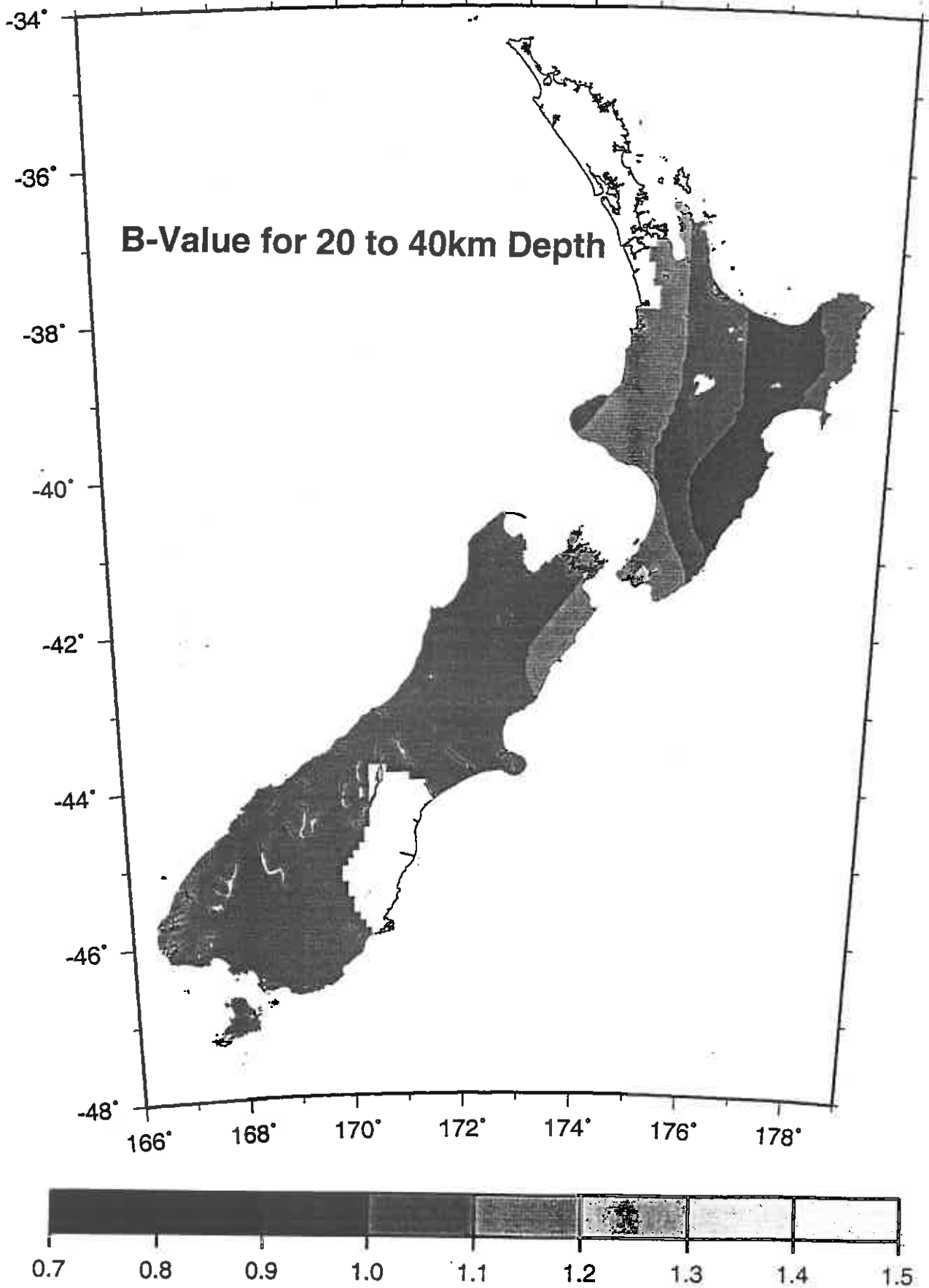


Figure 4h

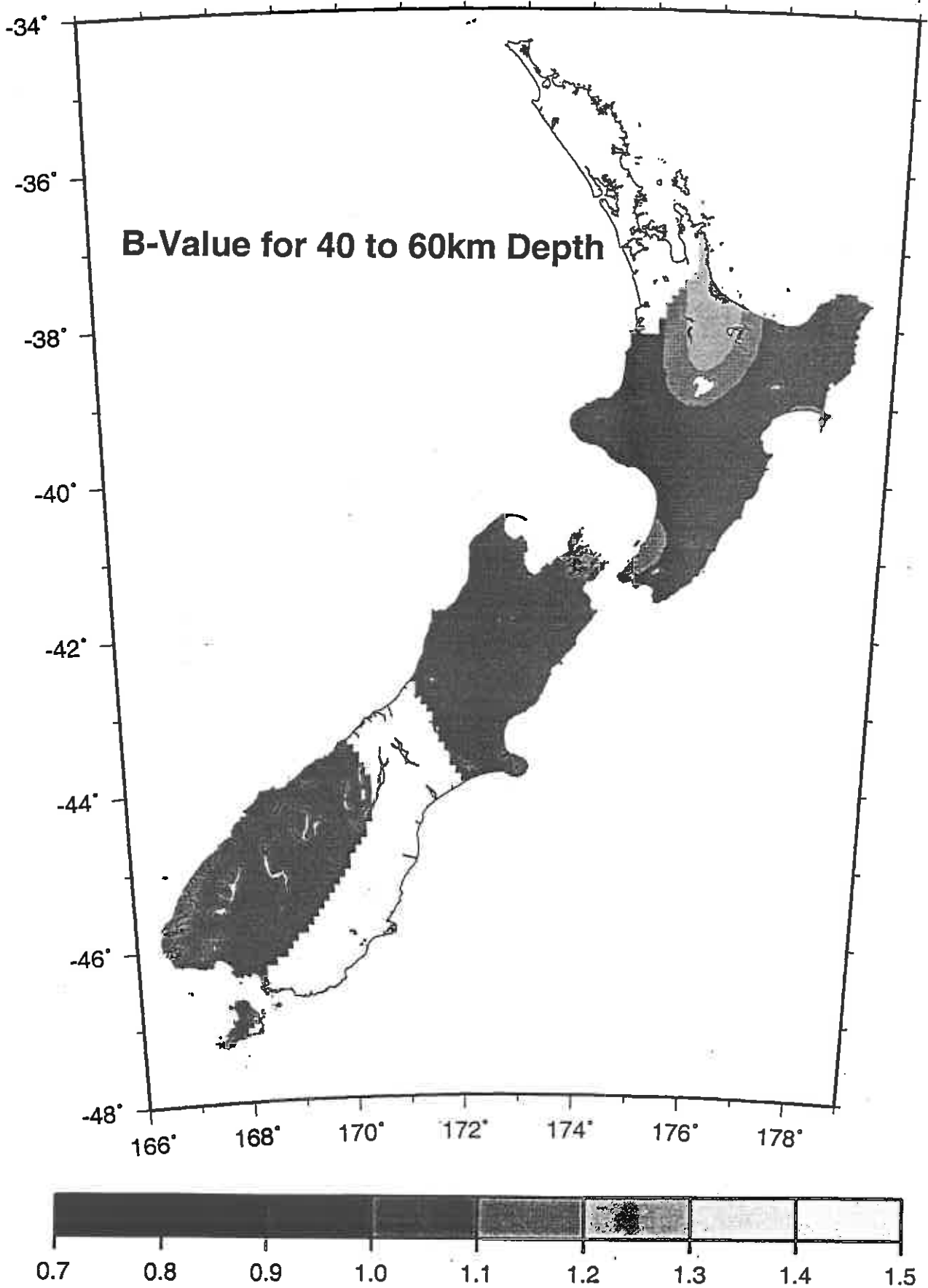


Figure 4i

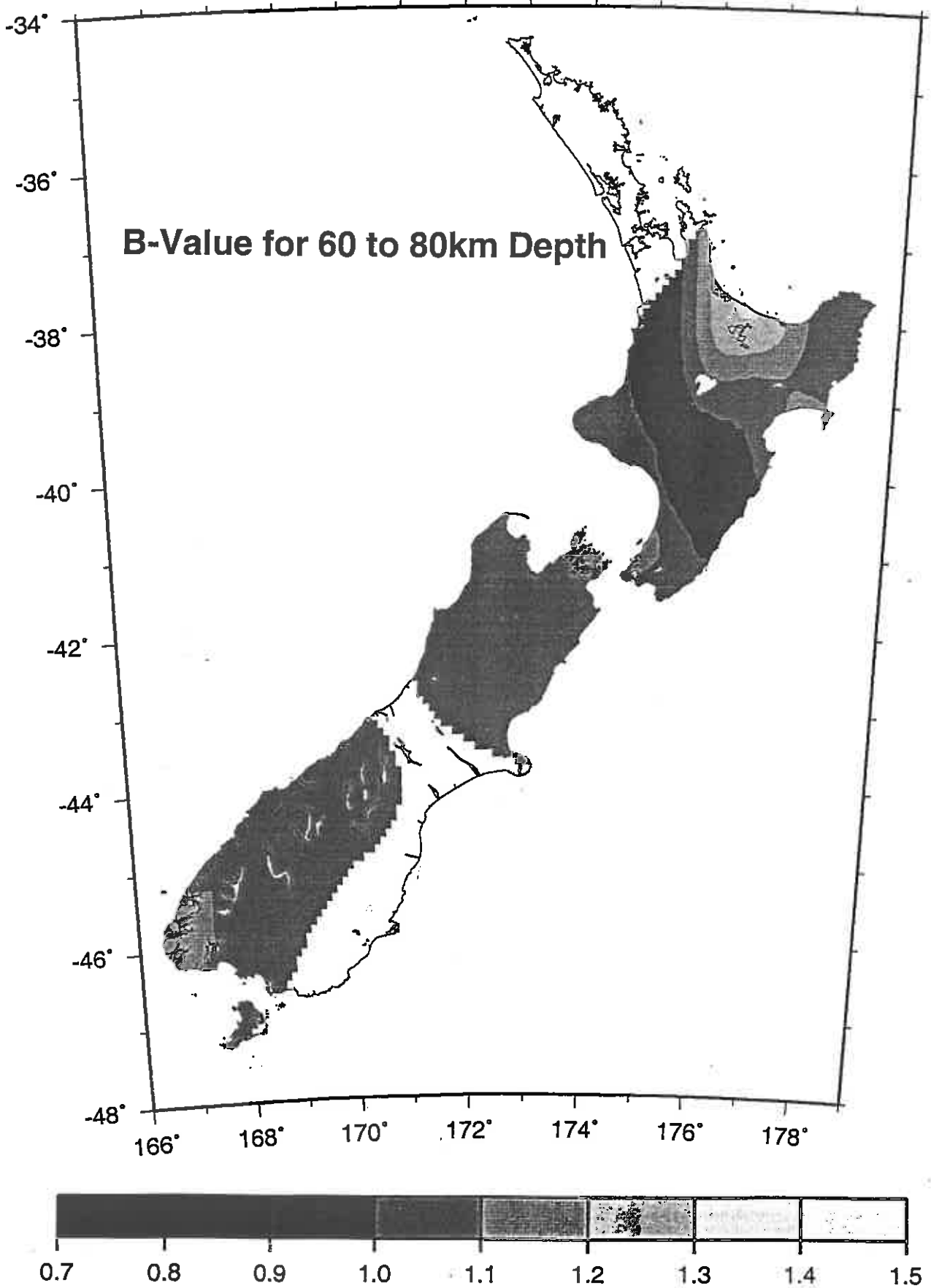


Figure 4j

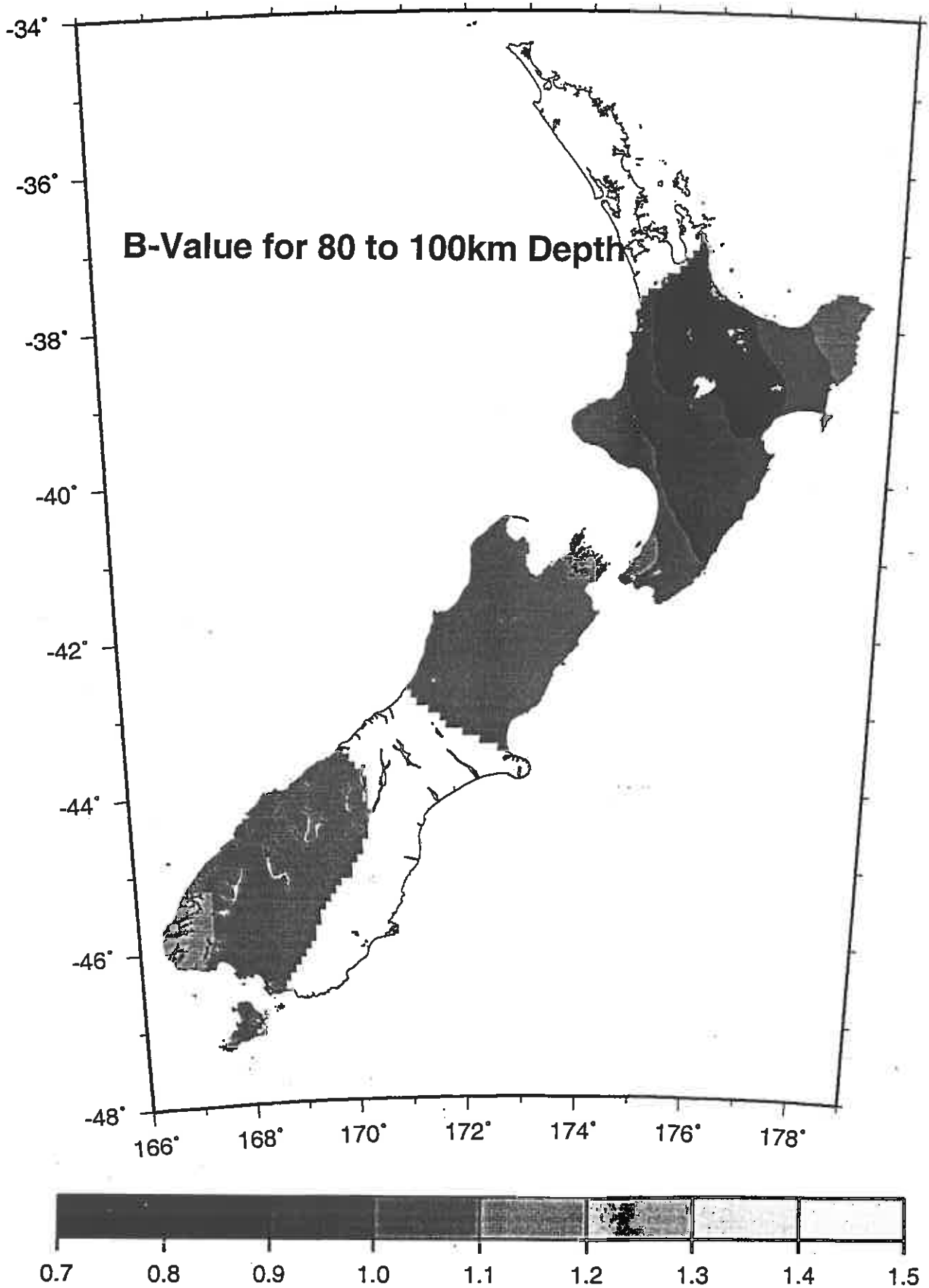


Figure 4k

